H2020 - GV-6 – 2017

This project has received funding from European Union's Horizon2020 Programme for research and innovation under grant agreement No. 770019.

Physical integration of hybrid and electric vehicle batteries at pack level aiming at increased energy density and efficiency Innovation Action (IA)

Grant Agreement — 770019

GHOST

InteGrated and PHysically Optimised Battery System for Plug-in Vehicles Technologies

D 4.1 Methodology test, characterization test and electro-thermal battery model report

DOCUMENT INFORMATION

Confidential

Report Document Template - Subject	
Authors	Joris Jaguemont VUB, Noshin Omar VUB, Theodoros Kalogiannis VUB, Sazzad Hosen VUB, Giorgio Mantovani IVECO, Michele Gosso CRF, Andreas Koenekamp AVL, Elise Nanini-Maury LBE, Iñigo Ondara IKERLAN, and Cristoph Unterrieder IFAT.
Nature	Document
Status	Revision of the submitted version

Change History

Version	Date	Description	Issued by
1	03/09/2018	First draft	VUB
2	19/09/2018	Second draft	VUB
3	30/09/2018	Final draft	VUB
4	30/05/2019	Revision of the submitted version	VUB

Table of Contents

List of Figures

List of Tables

1 Introduction

The aims of the project include the design of a novel and modular battery system with higher gravimetric energy density up to 20% and an increase of the volumetric energy density of the battery system up to 30% in comparison to the market and to the previous pack assembled in the Ecochamps project (5.7 kWh as nominal energy). Moreover, it is proposed to develop a mass-producible innovative and integrated design solution to reduce the battery integration cost at least 30% through smart design. The design of novel prototyping, manufacturing and dismantling techniques, is aimed to benefit the next generation of lithium-ion battery systems.

New test methodologies and procedures are to be evaluated towards reliability, safety and lifetime of different battery systems. The modular battery system should demonstrate the ease of process for two target applications (BEV bus with ultrafast partial charge capability and PHEV).

On one hand, a dedicated test methodology will be developed to reflect the battery behavior as close to the reality. It will be based on different developed techniques:

- The experiences from the standardization organizations regarding batteries
  - such as IEC, ISO, SAE, JAR
- Measured real load profiles of batteries from electric vehicles heavy-duty vehicles, covered in WP2
- Characterization techniques
  - such as advanced pulse testing, recently optimized for batteries at VUB.

The latter one is a promising identification technique, which can be used online to determine parameters for advanced battery models and for the state of functions estimation.

On the second hand, a needed in-depth cell characterization will be conducted. It will provide a detailed understanding of the short- and medium term behaviour of the battery cells. This characterization will take into account the electric and thermal aspects of the cells as well as a statistical spread on battery cell behavior for the development process of the electrical and thermal models in Task 4.4. The electrical and thermal behavior of the battery cells will be investigated at different and well-selected operating conditions: in particular at different temperature levels, with different current rates and at different values of the state of charge. The models will be validated according to the requirement of Task 4.6.

Finally, the last task will consist in developing a dynamic electric-thermal battery model able to predict, accurately the electrical and thermal responses and behaviors of the battery cell under a wide range of stress conditions.

2 Development of test methodology for characterization of batteries

In the report D2.2, potential cells for designing the battery pack of the PHEV and eBus have been evaluated. Among all candidates, the mentioned LTO cell (Toshiba 23 Ah) meets all requirements for the PHEV, most requirements for the eBus application and some for a second use in the stationary application. Therefore, the test methodology and characterization will be focused on this selected cell.

2.1 Cell datasheet

In order to reflect the battery behavior as close to reality, a dedicated test methodology is developed based on the LTO 23Ah Toshiba cell. The characteristic of the prismatic LTO-based cell is reported in Table 1, while Figure 1 is a picture depicting the cell.

	Toshiba 23Ah
Material	
Chemistry	LTO
Shape	Prismatic
Voltage	
Nom. Voltage (V)	2.3
End of charging voltage (EOCV V)	2.7
End of discharging voltage (EODV)	1.5
Energy	
Capacity (Ah)	23
Specific Energy (nominal - Wh/kg)	96
Energy Density (nominal - Wh/L)	202
Current DCH	
Continuous rms DCH (A)	93 – 4C
max DCH pulse **10s** (A)	184 - 8C
Current CHA	
Continuous rms CHA (A)	184 – 8C
max CHA pulse **10s** (A)	
max CHA pulse **60s** (A)	
Fast charge max **360s** (A)	184 - 8C

Mechanical	
Weight (kg)	0.550
Volume (L)	0.260
Dimensions LxWxH (mm)	115*22*103
Cost	
Price per piece (€/ piece)	41.2

Table 1. LTO 23Ah Toshiba cell characteristics

Figure 1. LTO 23Ah Toshiba cell

2.2 Characterization protocol

One of the main objectives of this test methodology is to secure the development process of the electrical and thermal models in Task 4.4 and lifetime model in Task 4.5. The development process of battery modeling consists of a series of standard testing procedures used for many years in the automotive industry in order to capture efficiently the electrical and thermal behaviors. Table 2 gives an overview of the available standard

testing procedures for specific tests for reviewing the characteristics and performance parameters of lithium-ion batteries for BEV and for HEV applications.

Test item	Test	Condition	Pack/System ISO/CD 12405-1/2	Extended	Cell IEC 62660-1	Extended
Pre-conditioning	Cycling	Temperature	25 °C		25 °C	
		Charge	standard charge		Standard Charge	
		Discharge	2C		0.2C	$2I_t$
		# Cycles	5		5	
Energy and capacity	CC discharge	Temperature	−18 °C, 0 °C, 25 °C, 40 °C		−20 °C, 0 °C, 25 °C, 45 °C	
		Charge	standard charge	# I_t-rates until max charge I_t-rate (as $1/3I_t$, $1I_t$, $2I_t$, ...)	standard charge	# I_t-rates until max charge I_t-rate (as $1/3I_t$, $1I_t$, $2I_t$, ...)
		Discharge	1C, 10C, 20C, I_{max}	$1/3I_t$, $2I_t$, $5I_t$	1C, 10C, 20C, I_{max}	$1/3I_t$, $2I_t$, $5I_t$
		# cycles	2		2	
Power and resistance	Pulse charge/ discharge	Temperature	−18 °C, 0 °C, 25 °C, 40 °C		−20 °C, 0 °C, 25 °C, 45 °C	40 °C instead of 45 °C
		Discharge	I_{max}, dis	$1/3I_t$, $2I_t$, $5I_t$, $10I_t$	0.2C, 1C, 5C, 10C	$1/3I_t$, $2I_t$, I_{max}
		Duration	0.1 s, 2 s, 10 s, 18 s		10 s	
		Charge	0.75*I_{max}, dis	$1/3I_t$, $2I_t$, $5I_t$, $10I_t$, I_{max}	1/3C, 1C, 5C, 10C	$2I_t$, I_{max}
		Duration	0.1 s, 2 s, 10 s		10s	
		SoC	80%, 65%, 50%, 35%, 20%		50%	80%, 65%, 35%, 20%
Energy efficiency	Pulse charge/ discharge	Temperature	0 °C, 25 °C, 40 °C	−18 °C	−20 °C, 0 °C, 25 °C, 45 °C	40 °C instead of 45 °C
		Discharge	See sequence in Table 4	$1/3I_t$, $1I_t$, $2I_t$, $5I_t$, $10I_t$, I_{max}	1/3C, 1C, 5C, 10C	$2I_t$, I_{max}
		Duration		10s	10s	
		Charge	See sequence in Table 4	$1/3I_t$, $1I_t$, $2I_t$, $5I_t$, $10I_t$, I_{max}	1/3C, 1C, 5C, 10C	$2I_t$, I_{max}
		Duration		10 s	10 s	
		SoC	65%, 50%, 35%	80%, 20%	50%	80%, 65%, 35%, 20%

Table 2. Overview of the defined tests in the standard ISO/CD 12405 ½ and IEC 62660-1

2.3 Electrical characterization

The electrical characterization of the cells is performed by implementing a characterization testing scheme derived from Table 2 and composed of the following subsequent characterization tests:

- Pre-conditioning
- Discharge Capacity test
- HPPC test
- OCV test

- Validation test
- EIS test

Almost all of the tests will be conducted at different temperatures in order to have a wide range of mobility for the model. The testing temperatures are selected in order to have different conditions and to represent the cell in extreme environmental conditions. A set of 3 cells for each temperature will be characterized for accuracy, performing different tests at:

- 0°C and 10°C for low-temperature environment
- 25°C for ambient temperature environment
- 35°C and 45°C for high-temperature environment
- Extreme low-temperature (-15°C) will also be investigated if timing allows it.

Then, while performing the second-life evaluation for stationary application, this set of tests will be redone on aged cells at 25°C.

The next sub-sections are dedicated to the description of each of these listed tests.

2.3.1 Pre-conditioning

The pre-conditioning test consists of a number of discharge and charge cycles of the battery to prepare the battery (initiating Lithium/electron flow) for future testing procedures. Additionally, through this test, the first initial capacity value of the battery is calculated. The test is performed at controlled ambient temperature (25°C) and starts with a status check of the battery, continuing with a standard charge at constant current followed constant voltage phases (CCCV) and discharge with constant current (CC). It continues by charging and discharging for 3 times in a row. The C-rates (or It) are a compromising value between time and degradation. Each time a discharge or charge is finished, a 3h pause is implemented. The pre-conditioning test is described below:

Pre-con Test			
Step	**Action**	**C-Rate**	**Limit**
		LTO	
1	Tempering		3h
2	Standard charge	1C	> EOCV <0.05 C-Rate
3	Pause		3h

4	Discharge	1C	EODV
5	Pause		3h
Steps 1-5 are repeated 3 times			

Table 3. Preconditioning test sequence

2.3.2 Discharge capacity test

The objective of this test is fairly straightforward. The discharged cell capacity expressed in Ah at different discharge C-rates (or It) and temperatures are obtained from the test results. Basically, it consists of performing full charges and discharges at different C-rates to obtain stable capacity measurements. This test is an important step as this capacity value is the reference value used for the other tests composing the characterization testing procedures. In addition, the C-rates chosen in this test are also used in the next tests.

The “Discharge Capacity test” is conceptually described below:

Capacity Test			
Step	**Action**	**C-Rate**	**Limit**
		LTO	
1	Tempering	T = 0°C, 10°C, 25°C, 35°C and 45°C	3h
2	Standard charge	1C	> EOCV <0.05 C-Rate
3	Pause		30 min
4	Discharge	C/3; C/2;1C; 2C; 4C, 8C	EODV
5	Pause		30 min
Steps 1-5 are repeated for each T.			

Table 4. Discharge capacity test procedure

2.3.3 OCV vs SoC test procedure

In order to determine the relation between the open circuit voltage (OCV) and the state of charge (SoC) of the battery, the OCV-test is performed according to the description given here below.

The test profile consists of a complete charge following by a complete discharge of the cell in steps of 5% between 100% and 0% SoC window of the available discharge capacity of the battery at 1C. The capacity related to this C-rate will be already available from the calculation during the “Discharge Capacity Test” at the 1C discharge pulse for each temperature. After each step, a relaxation period of 3h has been implemented, as it can appear as long but necessary rest time for relaxation. The OCV value at that

specific SoC levels is then defined as the voltage at the end of the 3h-relaxation period. Then, the battery is completely discharged and a series of charge pulses are applied in order to have the discharging and charging OCV behaviors. The voltages during each rest period are recorded to establish the cell's OCV behavior. From these data, OCV against SOC values can be estimated by straight-line interpolation or by curve fitting through the measured data points. Based on the obtained OCV values, a look-up table can be generated for the prediction of the OCV in function of the battery SoC for future battery models.

Additionally, by performing this procedure during both discharging and charging, the entropic changes for the reversible heat generation can be investigated. [1].

OCV vs SOC			
Step	**Action**	**C-Rate**	**Limit**
		LTO	
1	Tempering	T = 0°C, 10°C, 25°C, 35°C and 45°C	3h
2	Standard charge	1C	> EOCV <0.05C-Rate
3	Pause	3 hours	
4	Discharge	1C	ΔDOD = 5%
5	Pause	3 hours	
6	Charge	1C	ΔDOD = 5%
7	Pause	3 hours	
For each T, repeat steps 4 - 5 until EODV and 8-9 until EOCV for each temperature			

Table 5. OCV vs SOC test procedure

2.3.4 qOCV vs SoC test procedure

In complement to the OCV vs SOC test, the quasi-OCV test is performed. The idea of this test is to measure the voltage against the SoC under very low current in order to get a voltage response close to the OCV values. The test profile consists of a standard full charge following by a complete discharge and charge of the cell at the C/25 C-rate.

The OCV test procedure is conceptually described in the table below:

Quasi-OCV Vs SOC			
Step	**Action**	**C-Rate**	**Limit**
		LTO	
1	Tempering	T = 0°C, 10°C, 25°C, 35°C and 45°C	3h

2	Standard charge	1C	> EOCV <0.05*C-Rate
3	Pause		30 min
4	DCH	C/25	EODV
5	Pause		3 Hours
6	CHA	C/25	EOCV
7	Pause		30 min

Table 6. Quasi-OCV Vs SOC test procedure

2.3.5 HPPC test procedure

The hybrid pulse power characterization (HPPC) test is intended to measure the battery impedance using a test profile that incorporates both discharge and charge pulses, as shown in Figure 2. The primary objective of this test is to establish the DC internal resistance of the three tested cells. The internal resistance is responsible for the irreversible heat generation and a measurable degradation is expected that increases its value at every SoC and C-rate. Hence, as a function of the SoC, of the current rate, and of the temperature, the internal DC resistance is determined on a large range of SoC points, currents, and temperatures.

The idea of this test is to apply a 10-second discharge-pulse and 10-second charge-pulse power capabilities at each given SoC and for different C-rates. A 600s-rest period is scheduled between each HPPC pulse. From the result data, an algorithm will afterward determine the DC internal resistance of the cell.

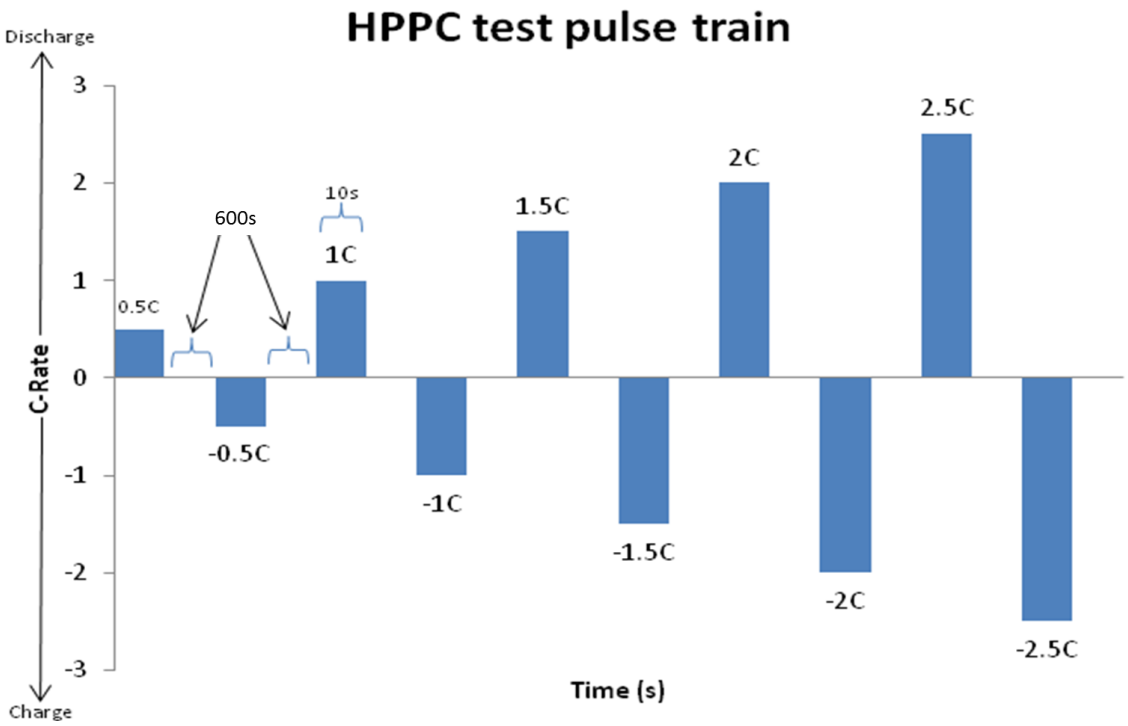

Figure 2. Example of an HPPC pulse train

The HPPC test procedure is conceptually described in the table below:

HPPC Test			
Step	**Action**	**C-Rate**	**Limit**
		LTO	
1	Tempering	T = 0°C, 10°C, 25°C and 45°C	3h
2	Standard charge	1C	> EOCV <0.05 C-Rate
3	Pause		3 h
4	Discharge	1C	ΔDOD = 5%
5	Pause		3 h
6			

HPPC		
Time (s)	Acc T (s)	**LTO**
10	10	C/3
600	610	PAUSE
10	620	- C/3
600	1220	PAUSE
10	1230	C/2
600	1830	PAUSE
10	1840	- C/2
600	2440	PAUSE
10	2450	1C
600	3050	PAUSE
10	3060	- 1C
600	3660	PAUSE
10	3670	2C
600	4270	PAUSE
10	4280	- 2C
600	4880	PAUSE
10	4890	4C
600	5490	PAUSE
10	5500	- 4C
600	6100	PAUSE
10	6110	8C
600	6710	PAUSE
10	6720	- 8C
600	7320	PAUSE

Repeat steps 3 - 6 until DoD 90%

Table 7. HPPC test procedure

2.3.6 Validation tests

In order to correctly validate the electrical models created based on the parameters acquired from the different characterization tests, some independent validation tests are additionally performed. These tests can be used to compare the output of the model with the voltage response of the cell.

The worldwide harmonized light vehicles (WLTC) test procedure has been selected in order to perform the validation of the electrical model. During the 1990s, the emergence of electric road vehicles powered by alkaline batteries pushed the development of suitable test procedures and standards. Conventional constant current discharge tests, as were defined for lead-acid batteries, did not reflect the actual use pattern of the batteries in electric vehicles. The WLTC test procedure used for electrical validation is based on the WLTC driving cycle that was developed in collaboration of the EU, Japan, and India under the guideline of UNECE World Forum for Harmonization of Vehicle Regulations. In the framework of GHOST and Task 4.1, a current load profile representing a high-power application has been derived based on the WLTC driving profile as shown by Figure 3. This profile is meant for the PHEV case

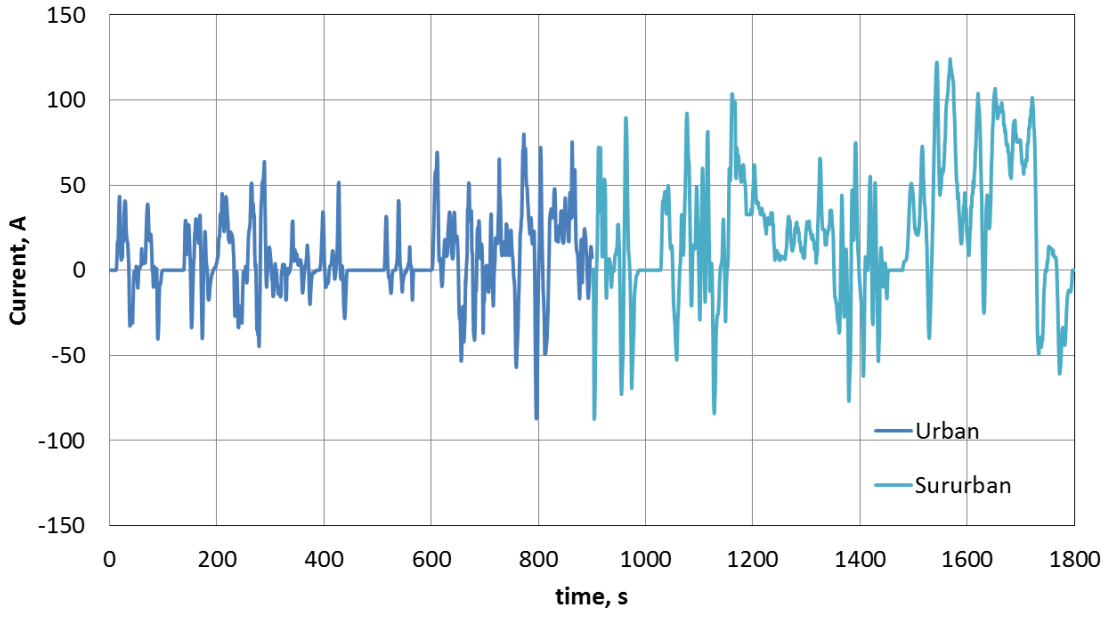

Figure 3. WLTC driving profile

The WLTC validation consists of standard charge procedure followed by the continuous repetition of WLTC current load profile as shown by the example in Figure 4.

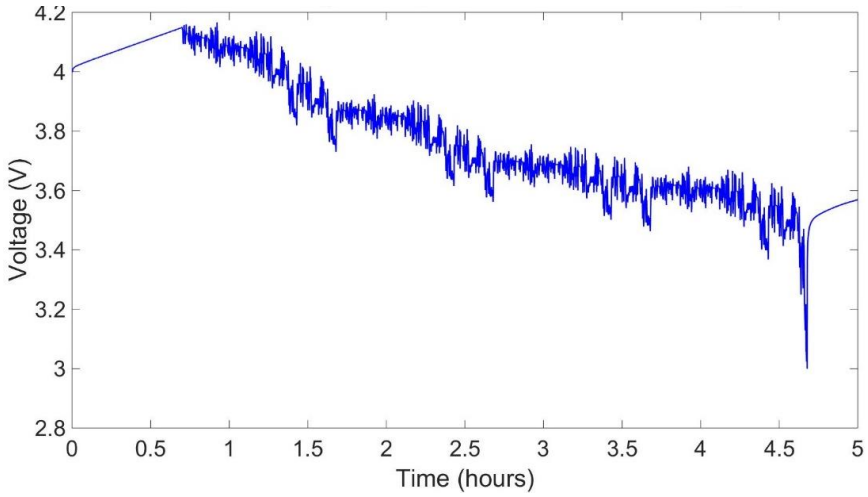

Figure 4. WLTC profile with repetition for a sample cell at 25 degrees

Electrical validation Test			
Step	**Action**	**C-Rate**	**Limit**
		LTO	
1	Tempering	T = 0°C, 10°C, 25°C, 35°C and 45°C	3h
2	Standard charge	1C	> EOCV <0.05 C-Rate
3	Pause		30 min
4	DCH	1C	ΔDOD = 5% to 90%SoC
5	Pause		30 min
6	Cycle	WLTC	From 90%SoC to 10%SoC
7	Pause		30 min
Steps 2-7 are repeated three times for accuracy and for each T			

Table 8. Electrical validation test procedure

2.3.7 EIS tests

The purpose of the EIS tests is to build a comprehensive database which can be used in order to derive reliable temperature estimation methods form the measurement of the cell AC impedance. Nevertheless, low-frequency points of the spectrum will also be collected for SOH studies. The estimation techniques should cover the following aspects:

- Different charge/discharge current rates, relaxation
- Different temperature imposed from outside
- Temperature transients due to self- heating in charge/discharge
- Different SOC levels
- Aging of the cell (tracking of the estimation method along the cycles)
- Different cell samples

The selected cells do not allow direct sensing of the internal temperature. Temperature sensors will be placed on the cell surface. The location of the thermocouple is discussed in the next section.

The figure below shows the test sequence that will be implemented in order to create the database.

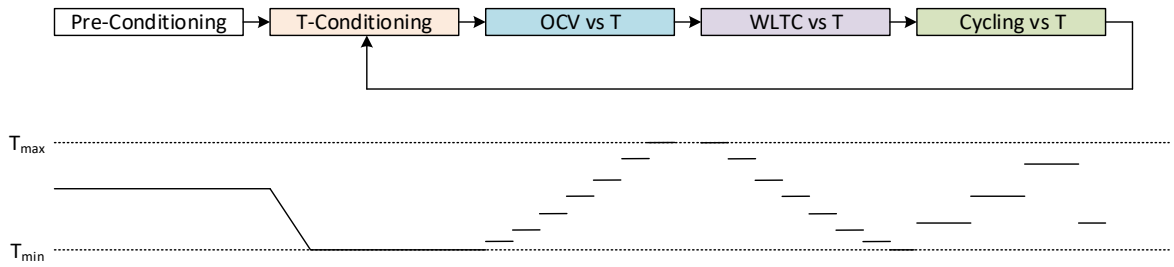

Figure 5. Measurement sequence for EIS

A set of new cells (8) are first pre-conditioned as in 2.3.1. Then the following test sequence is repeated:

- OCV test – as described in 2.3.3. The same temperature range will be used: 0, 10°C, 25°C, 35°C, and 45°C. Full spectrums are collected during the measurement .During charge and discharge, the spectra are collected continuously. During relaxation periods every 10 minutes.
- Checkpoint 1 – collected data is checked in order to find a target temperature estimation method
- Driving Test WLTC as in 2.3.6. In this case, the charge/discharge current cannot exceed the 100A due to the limitation of the IFAT lab equipment. Depending on the estimation method selected, a reduced number of frequency points (max 4) is continuously measured.

- Checkpoint 2 – the data is analyzed and the estimation method is checked against the measured temperature. If needed the Driving test is repeated on different frequency points.
- Cycling – the purpose of the Cycling tests is to age the cells. Cycling is performed until the targeted total number of cycle is reached (targeted total number of cycles is defined to be 100 for D4.1, for cycling over a higher number of cycles – for aging considerations - it is referred to D4.2). The basic cycle is the pre-conditioning cycle of 2.3.1. The temperature is set to 0°, 25° 35°C 45°C. The discharge cycle is run at 0.5C/ 1C / 2 C before the temperature is changed (roughly 30 cycles per temperature). The cycling stops as soon as the target number of the cycle for the cells is reached.

The table below adds to the description of the previous tests (2.3.1, 2.3.3, 2.3.6), the description of the additional EIS tests, in terms of frequency range and time interval. The excitation current amplitude will be within -100mA and -500mA average.

EIS test				
Step	**Test type**	**Action**	**Frequency steps**	**Repetitions**
1	OCV vs. SOC	Tempering	whole spectrum (1Hz - 5kHz)	10min
2	OCV vs. SOC	Standard Charge	whole spectrum (1Hz - 5kHz)	continuously
3	OCV vs. SOC	Pause	whole spectrum (1Hz - 5kHz)	10min
4	OCV vs. SOC	Standard Discharge	whole spectrum (1Hz - 5kHz)	continuously
5	OCV vs. SOC	Discharge	whole spectrum (1Hz - 5kHz)	continuously
6	OCV vs. SOC	Charge	whole spectrum (1Hz - 5kHz)	continuously
7	WLTC vs. T	Tempering	whole spectrum (1Hz - 5kHz)	10min
8	WLTC vs. T	Standard Charge	max. 4 frequency points	continuously
9	WLTC vs. T	Pause	whole spectrum (1Hz - 5kHz)	10min
10	WLTC vs. T	Discharge	max. 4 frequency points	continuously
11	WLTC vs. T	Cycle	max. 4 frequency points	continuously
12	Cycling	Tempering	whole spectrum (1Hz - 5kHz)	10min
13	Cycling	Standard Charge	max. 4 frequency points	continuously
14	Cycling	Pause	whole spectrum (1Hz - 5kHz)	10min
15	Cycling	Discharge	max. 4 frequency points	continuously

Table 9, EIS test protocol

2.4 Thermal characterization

The thermal characterization of the cells is performed by implementing a characterization testing scheme derived from Table 2 and composed of the following subsequent characterization tests:

- Thermal heat capacity test
- Thermal conductivity test
- OCV thermal test
- Validation test

The next sub-sections are dedicated to the description of each of these listed tests.

2.4.1 Temperature measurement

For every test, a maximal allowable temperature is defined to prevent gassing and critical failure of the cell resulting from overheating and thermal runaway. Also, the evolution of the temperature is an important parameter for designing a thermal model. Thus, it is necessary to have a reliable way of measuring battery temperature.

Because with the test equipment available, only one point of the battery can be measured for temperature, this point has to be carefully chosen. To select the right temperature point, IR images of the cell will be captured by a Ti25 thermal imager (FLUKE®, Everett, WA, USA) at regular time intervals during a high-current discharge capacity test (4C or 92A). The IR thermography will show the highest temperature point of the cell for which the thermocouple will be placed.

2.4.2 Thermal heat capacity test

Adiabatic calorimetry will be used as the method for heat capacity measurements. This method consists of heating one cell with a known amount of power supplied by a planar resistance placed between them in an adiabatic environment provided by an accelerating rate calorimeter. This value is responsible for the heat accumulation inside the cell, but it is not expected any big variation of its value due to aging or SoC changes.

The heat capacity test consists of performing different external heating tests in order to evaluate the temperature increase of the cells when no heat is lost to the surrounding area. All the supplied heat is ideally accumulated in the cell's body. By knowing the mass of the cells and the voltage and current supplied to the heater, the heat capacity value can be calculated at any temperature or over any temperature range as:

$$C_p = \frac{Q}{m\Delta T} \tag{1}$$

where C_p is the specific heat capacity (kJ/kg.K), Q the heat generation rate (W), m the mass of the cell (m) and ΔT the temperature difference.

2.4.3 Thermal heat conductivity assessment

Most of the reported methods of thermal conductivity characterization are generally extensive, cost-intensive and cell destructive. Therefore, the conductivity coefficients will be directly obtained from a parameter estimation technique for which the experimental and simulation results will be compared. Then, through an iterative methodology, it will find the most appropriate value to match the experimental and simulation results and gives a good estimate of the parameters. Nonetheless, the values will be compared to the ones that Toshiba provided.

2.4.4 OCV thermal test

In order to determine the variation of the entropic heat coefficient with the SOC, the OCV measurements will be performed over the whole SOC interval by considering a 10% SOC resolution (10%:10%:90%). An example of the thermal cycle used during the test is shown in Figure 6. Basically, it consists of performing OCV measurements at different temperatures to see their derivative relation at different SOC levels. The SOC level is changed with 10% of variation due to the very non-linear nature of the variable. Then the thermal cycle is performed to obtain a reliable mean variation of the OCV with the temperature steps.

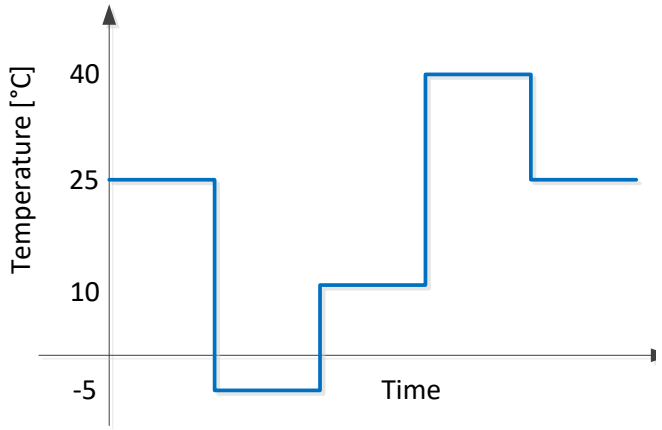

Figure 6. Example of a thermal cycle.

The voltage will be recorded during each of the tests at different SOCs. The entropy coefficient at each SoC, is given by the slope dU^{avg}/DT =A where V = f(T)=A T+B with V in [V] and T in [K]. After that the $dU^{avg}/dT=g(SoC)$ will be obtained.

For comparison, the OCV measurements performed for the electrical characterization will be used.

2.4.5 Validation tests

In order to correctly validate the thermal models created based on the parameters acquired from the different characterization tests, two independent types of validation tests are additionally performed: the constant current and dynamic current test. These tests can be used to compare the output of the model with the temperature response of the cell.

The constant current validation test consists of discharging and charging profiles at high C-rates and 100% SOC levels will be performed using the cells. To ensure the maximum heat generation, a discharging current of 4C (92A) will be applied.

The dynamic validation consists of using the same Driving Test WLTC as for the electrical characterization.

Thermal validation test			
Step	**Action**	**C-Rate**	**Limit**
		LTO	
1	Tempering	T = 0°C, 10°C, 25°C and 45°C	3h
2	Standard charge	1C	> EOCV <0.05 C-Rate
3	Pause		30 min
4	DCH	4C / dynamic profile	to 0%SoC
5	Pause		30 min
Steps 2-5 are repeated three times for accuracy			

Table 9. The thermal validation test procedure

2.5 Text matrix for electro-thermal characterization

A summary of the testing procedure can be found in the test matrix reported below:

Electrothermal matrix					
Temperature (°C)	45				
Type of test	Capacity	OCV	qOCV	HPPC	Validation test
Number of cells	4				
Temperature (°C)	35				
Type of test	Capacity	OCV	qOCV	HPPC	Validation test
Number of cells	4				
Temperature (°C)	25				
Type of test	Capacity	OCV	qOCV	HPPC	Validation test
Number of cells	4				
Temperature (°C)	10				
Type of test	Capacity	OCV	qOCV	HPPC	Validation test
Number of cells	4				
Temperature (°C)	0				
Type of test	Capacity	OCV	qOCV	HPPC	Validation test
Number of cells	4				
Total cells	10				

Legend	
Capacity	Multiple capacity tests done at different c-rates (typically 2C, 1C C/2, C/3, C/5)
HPPC	Hybrid pulse power characterisation for internal resistance assessment
OCV	Open circuit voltage for open voltage assessment
qOCV	quasi-Open circuit voltage for SOC and OCV relationship
Validation test	Dynamic test to validate the electrical model / high current tests to validation the thermal model

Table 10. Text matrix for electro-thermal characterization

2.6 Aging characterization

The aging characterization of the LTO will be explained in more details in the D 4.2 Ageing (calendar and cycling) analysis and lifetime model report. Nonetheless, since all the three aspects (thermal, electrical and aging) are linked, the aging test matrix and the common points will be briefly discussed.

In order to characterize the lifetime behavior of the LTO cell, a large test-matrix including various combinations of cycling temperatures, DoD-levels and charge and discharge current rates is developed and each test condition will be carried out on at least 3 cells. An overview of this test-matrix is given in Table 11 where the numbers indicate the

number of cells subjected to each cycling condition. All different conditions and specific testing will be fully detailed in D4.2 but a short remark can be done.

Regarding the influence of the charging-discharging current on the lifetime of the cell, the minimum, and maximum C-rate conditions should match the boundaries of the electrical characterization, otherwise, discrepancies might happen and temper with the efficiency of the model. This means that the lifetime model should be based on those limits.

Moreover, in order to have a more representative lifetime behavior aspect, a condition for which 8C (184A) has been identified as important for the project.

Cycling Matrix

DOD			100			60			40			20			
Mid-SOC			80	50	20	80	50	20	80	50	20	80	50	20	
Temperature (°C)	Charge (C-rate)	Discharge (C-rate)													Total cells
0	1C			3											3
10	1C			3			3						3		9
25	1C	1C		3			3		3	3	3	3	3	3	24
	1C	2C		3											3
	2C	2C		3											3
	4C	1C		3											3
	8C	1C		3											3
35	1C	1C		3											3
45	1C			3			3					3			9
Total cells			27			9			3	3	3	6	6	3	60

Calendar matrix

Storage-SOC	100	80	50	20	
Temperature (°C)					Total cells
10		3	3	3	9
25	3	3	3	3	12
45		3	3	3	9
Total cells	3	9	9	9	30

Total cells	90

Legend	
	100/50 1C 1C is the base case, shared for all temperatures so we can calculate temperature influence
	Simulating "Cold start", load cycles at high mid-SOC
	Simulating cold environnement, load cycles at 10°C
	Influence of discharge and charging current rate, only at 25 deg
	Baseline of tests, this will provide the influence of DOD and Mid-SOC, which we will transform to different temperatures, using the base case
	Effect of Fast-Charging (one 100% charge, one partial charge)
	High-temperature cycling, both high and medium-depth

Legend	
	High-SOC storage influence to compare with cycle ageing
	Base-case for comparing different temperatures and SOC
	Low-SOC storage influence

Table 11. Overview of the aging test matrix.

3 Electro-thermal characterization results of LTO cells

A set of 10 cells has been characterized by performing different tests described in the section earlier. In this section, the electrical and thermal results are presented.

3.1 Results from standard data collection for electrical modeling

3.1.1 Results from the pre-conditioning

The pre-conditioning test consists of a number of discharge and charge cycles of the battery to prepare the battery (initiating Lithium/electron flow) for future testing procedures. 3 cycles were done at 25°C and using for both charge and discharge part at 1C before the dedicated electrical characterization tests were performed. The voltage range was 2.7V – 1.5V in accordance with the specifications of the cell manufacturer.

This was done to ensure the formation of the cell. An example of the voltage evolution during the preconditioning test is shown in Figure 7.

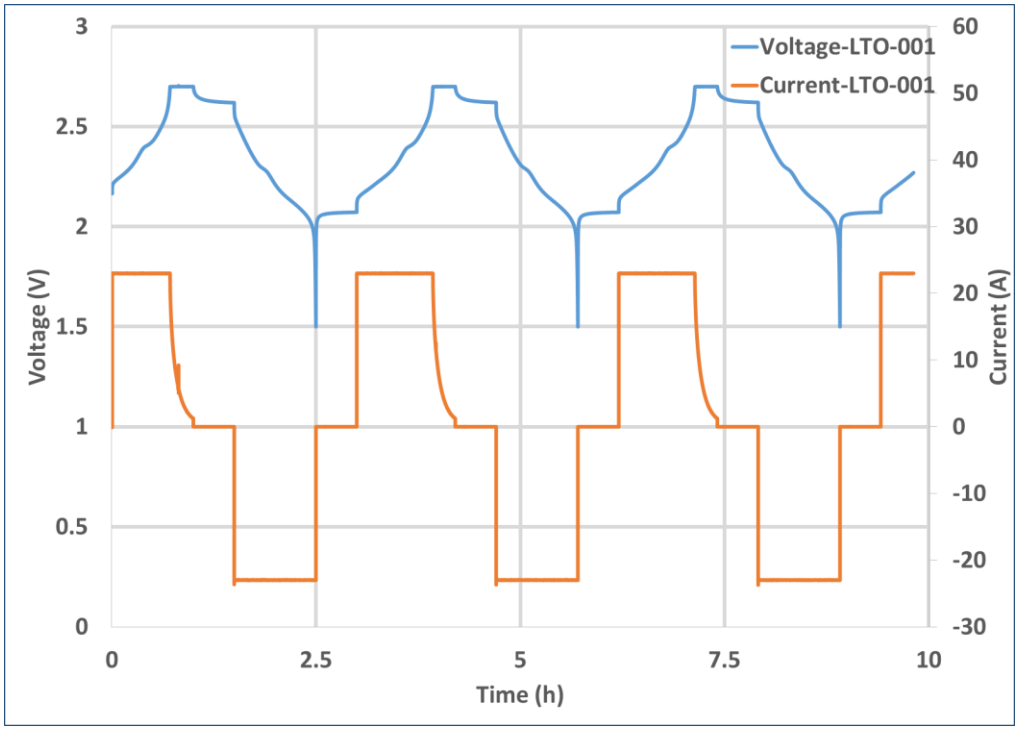

Figure 7. Preconditioning at 25°C at 1C.

3.1.2 Results from the advanced capacity test

As mentioned in the overview the cells at different temperatures were charged at a 1C rate and then discharged at C/3; C/2; 1C; 2C; 4C, and 8C respectively. The results for one of the cells at various temperatures is shown in Figure 8 to Figure 10, below. Table 12 and Table 13 report the charge capacity, the energy density and the discharge capacity of the LTO-based cell at different temperatures and different low C-rates. The specific discharge energy was calculated by using the discharge energy delivered from the discharge capacity test over the mass of the cell, 0.550g (provided by the manufacturer). A general increasing trend of the capacities can be observed with increasing temperatures which could be explained by kinetics at higher temperatures. Moreover, the capacity values are lower when the C-rate is increasing which is in accordance with the Peukert's Law [2]. However, at low temperatures, the capacity values are lower with a decreasing C-rate, this is due to the sluggish electrochemical reaction resulting from the low-temperature which is blocking the cell capacity. This justifies why at higher C-rates, due to the produced heat from self-heating [3], [4], the capacity values are higher. In addition, the values obtained by the experiment are very close to the manufacturer quoted data which shows the solid accuracy of the data displayed in this report.

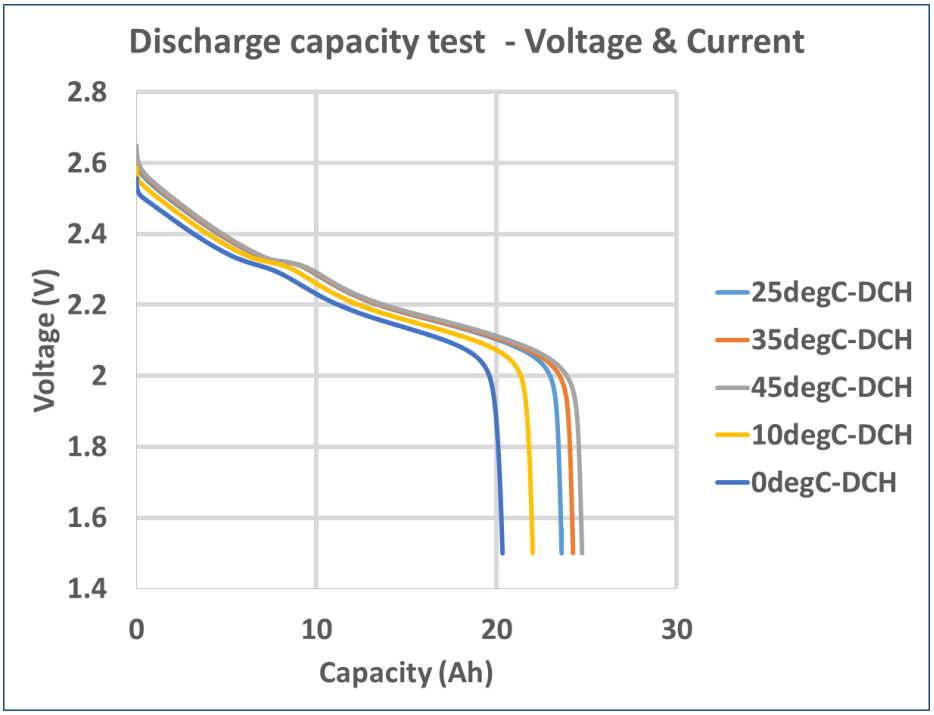

Figure 8. Discharge capacity tests at different temperatures at C/3.

Figure 9 shows the energy density calculated from the discharge capacity tests.

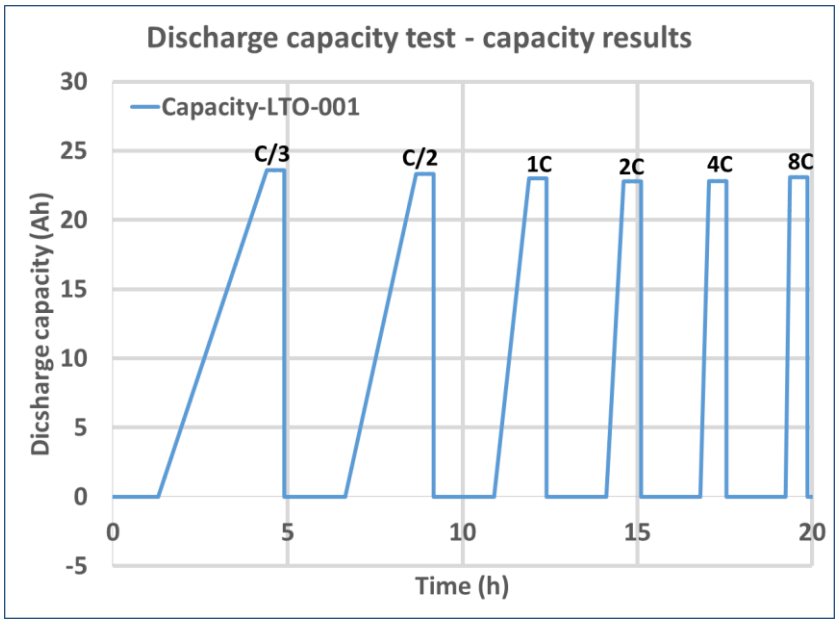

Figure 9. Discharge capacity tests at different c-rates at 25°C.

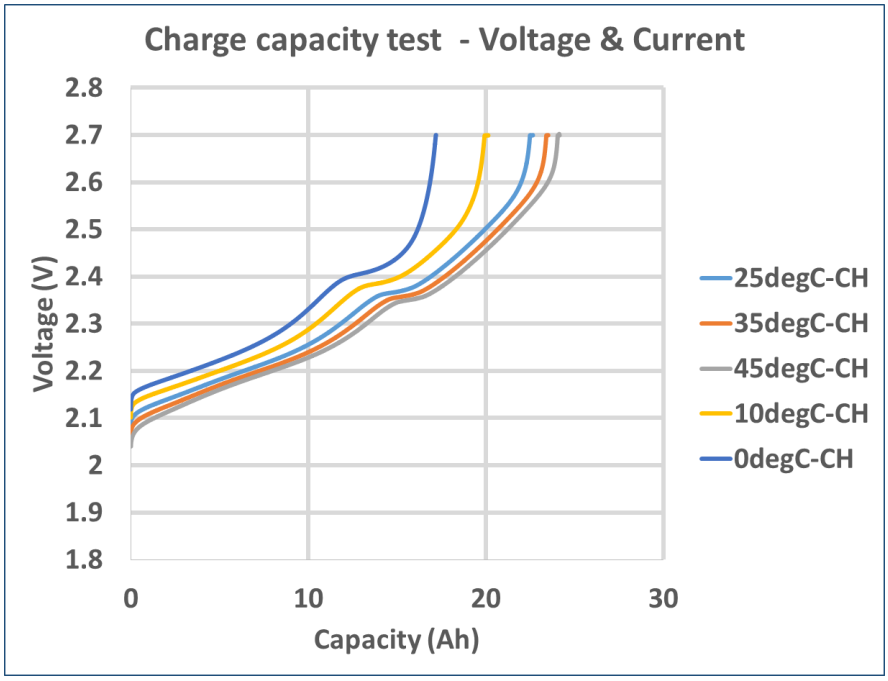

Figure 10. Charge capacity tests at different temperatures.

Table 12. Capacity values for different temperatures.

C-rate	C/2				
Temperature	0	10	25	35	45
Energy density (Wh/kg)	82	90	97	99	101
Charge capacity (Ah) – CC part	17	20	22.5	23.4	24

Table 13. Capacity values for different c-rates.

Temperature (°C)	25°C					
C-rate	C/3	C/2	1C	2C	4C	8C
Discharge capacity (Ah)	23.6	23.3	23.1	23	22.8	22.7
Charge capacity (Ah)	23.2	23.1	23	23	22.9	22.8
Temperature (°C)	35°C					

Discharge capacity (Ah)	24.2	23.9	23.7	23.6	23.5	23.4
Charge capacity (Ah)	24.2	23.9	23.7	23.6	23.4	23.4
Temperature (°C)	45°C					
Discharge capacity (Ah)	24.7	24.5	24.3	24.1	24	23.9
Charge capacity (Ah)	24.4	24.4	24.3	24.3	24.2	24.2
Temperature (°C)	10°C					
Discharge capacity (Ah)	21	21.23	21.6	21.7	21.8	21.9
Charge capacity (Ah)	21.2	21.21	21.3	21.4	21.7	21.8
Temperature (°C)	0°C					
Discharge capacity (Ah)	19.3	19.4	19.6	19.7	20.3	20.6
Charge capacity (Ah)	19.3	19.4	19.5	19.5	19.9	20.2

3.1.3 Results from the OCV test

Another important electrical characterization test is the “Open Circuit Voltage (OCV) test”. This test provides the open circuit voltage of the cell at different levels of the state-of-charge (SOC). The OCV curve was determined for both the charge and the discharge condition of the LTO-based cell and was determined at different values of the temperature.

OCV characterization for 25°C is shown in Figure 11 and OCV curves for all test is shown in Figure 12. It can be seen that the values at low and high SoC in the OCV characterization reflect clearly the non-linear voltage evolution. The values can be used for the electrical model for the battery voltage equation. Moreover, based on the obtained OCV values, a look-up table can be generated for the prediction of the OCV in function of the battery SOC for the electrical modeling part.

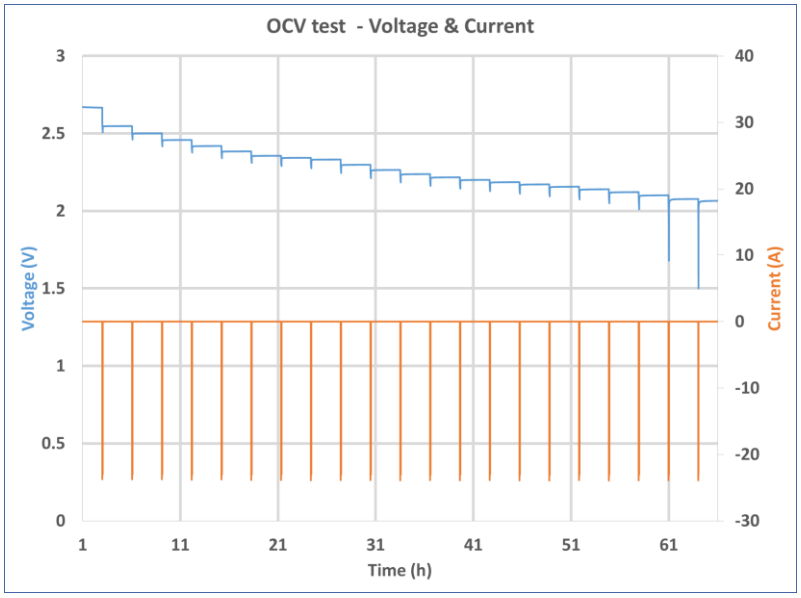

Figure 11. Discharge OCV test profile for the LTO Toshiba cells at 25°C.

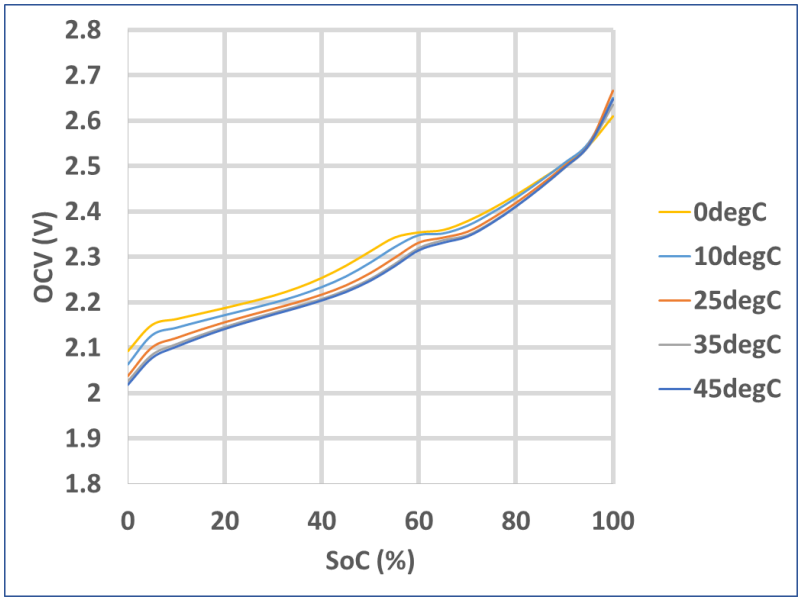

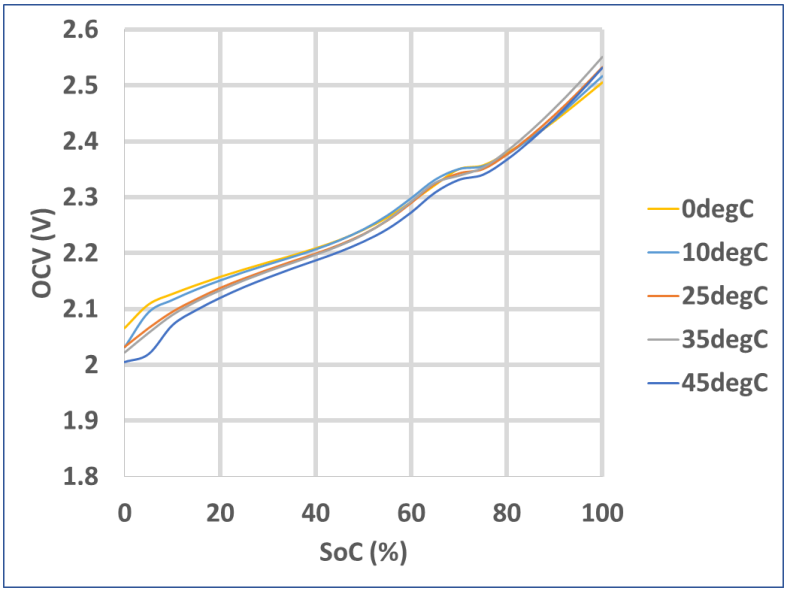

Figure 12: OCV curves of the NMC cell at different temperatures with discharge OCV curve (top) and charge OCV curve (bottom).

3.1.4 Results from the qOCV test

The qOCV tests were performed by the method mentioned in the previous section. The idea of this test is to measure the voltage against the SOC under very low current in order to get a voltage response close to the OCV values. The qOCV results at different temperatures are shown in Figure 13. It can be seen from the comparison with the normal OCV test that the values are pretty similar and that the temperature does not have a great impact on qOCV values between 0% and 90% SOC which is an acceptable upper range limit for the future electrical model.

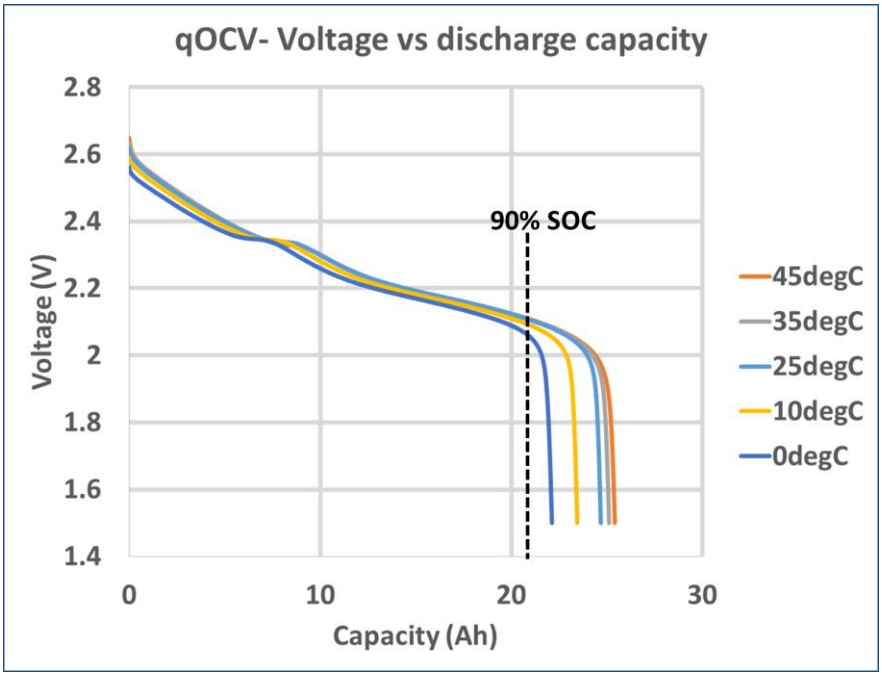

Figure 13. qOCV test results for one of the cells at 25°C.

3.1.5 Results from the HPPC test

The hybrid pulse power characterization (HPPC) test is intended to measure the battery impedance using a test profile that incorporates both discharge and regen pulses. The primary objective of this test is to establish, as a function of SOC, the internal resistance of the tested cell. A representative figure showing the current pulses implemented is shown in Figure 14. During the 10-sec charge and discharge pulses, extended voltage limits have been used: A preliminary simulation can be performed taking as validation profile the different pulses performed information to the model to simulate the behaviour of the studied lithium-ion cells and to extract the electrical parameters needed for the model (R_0, R_1, C_1, R_2, and C_2). The methodology for the extraction is explained in the next section.

The HPPC characterization result is shown in Figure 15, with the values of the discharge and charge internal resistance at C/5. As shown in this figure, the discharge internal resistance is higher at lower SoC levels and decreases with increase in SoC level. For the charging internal resistance, it is the opposite with a higher resistance value at high SoC. Moreover, one can see that the resistance during charge shows higher values than during discharge, this means that charging the cell and in particular from 80% to 100% can generate clearly unwanted heat and if not controlled, this can lead to hazardous runaways.

Regarding the temperature influence, the resistance values appear to be similar at higher temperature and for both states.

On the other hand, the resistance seems higher for both states at lower temperatures. This is due to sluggish electrochemical reactions occurring in cold weather that disable the Li-ion transfer and increase the resistance.

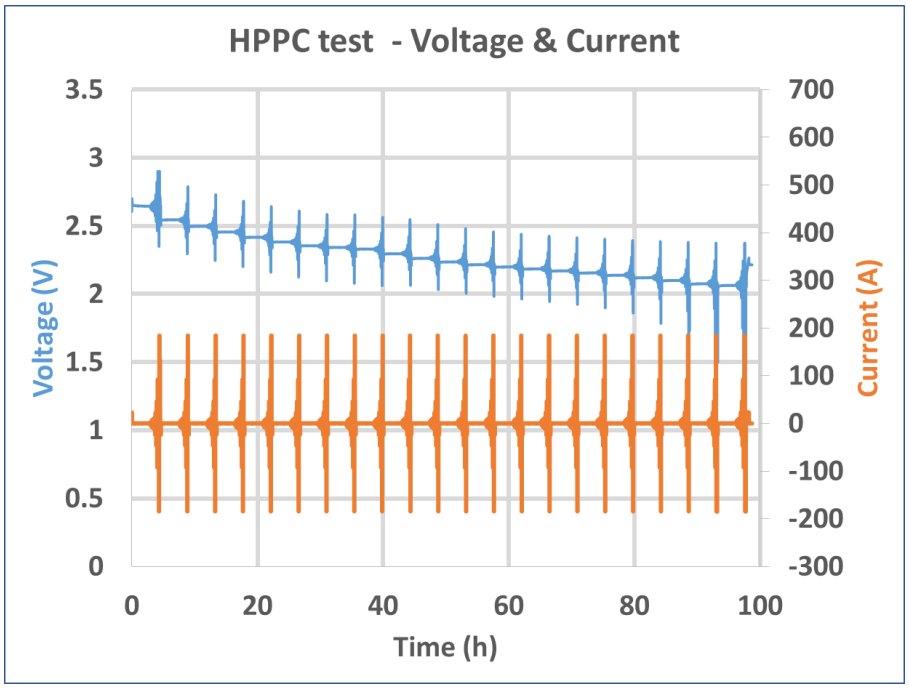

Figure 14. HPPC pulse train at 25°C with the current profile and voltage output response.

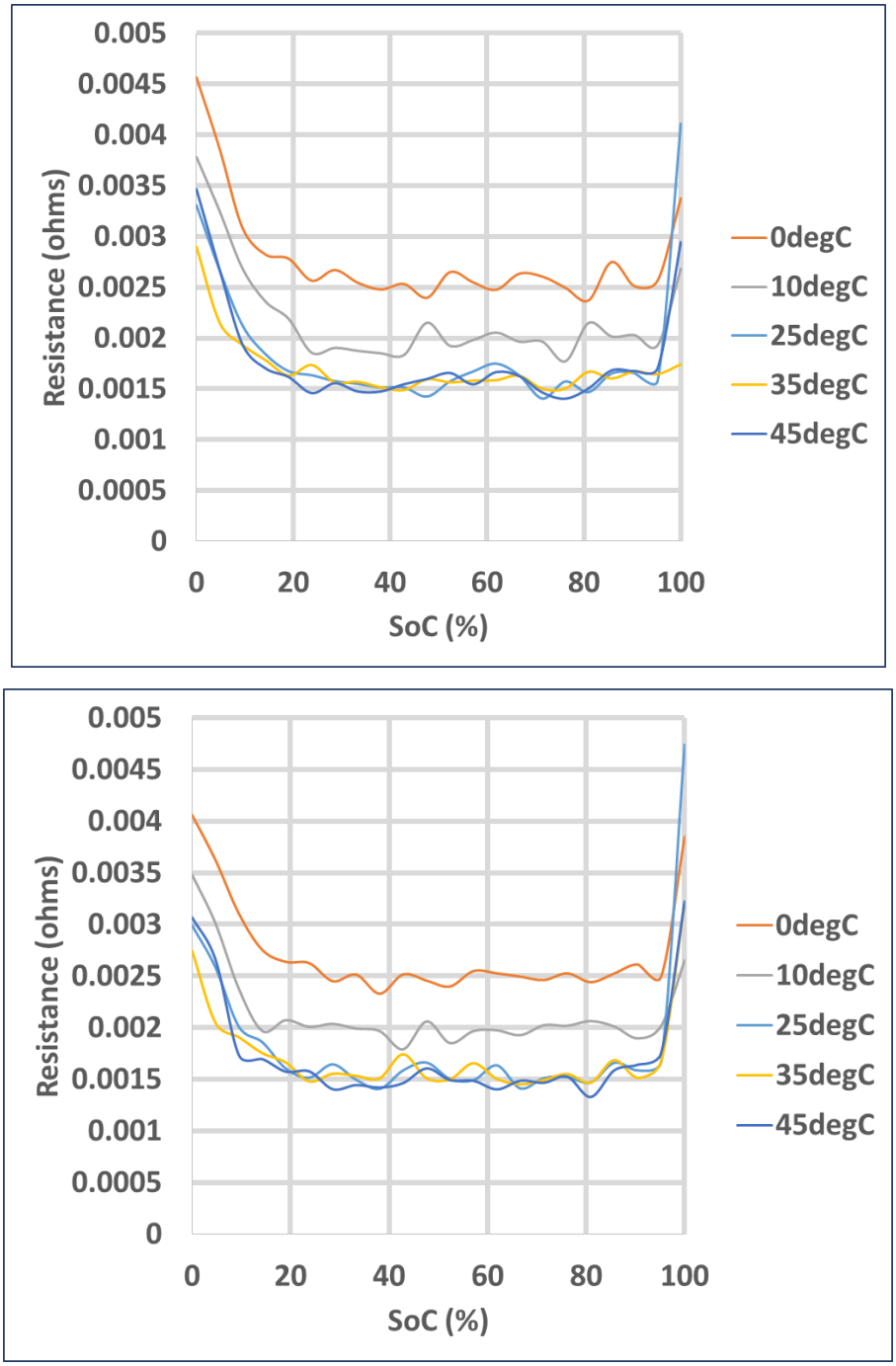

Figure 15. Internal resistance evolution at different temperatures for a discharging (top) and charging (bottom) state at C/5.

3.1.6 Results from the electrical validation tests

The WLTC profile used for validation is presented in Figure 16. The measured cell voltage response during this test will be compared to the simulated voltage of the cell in

the next section for validation purpose. This test has been performed at different temperatures for the complete validation of the model.

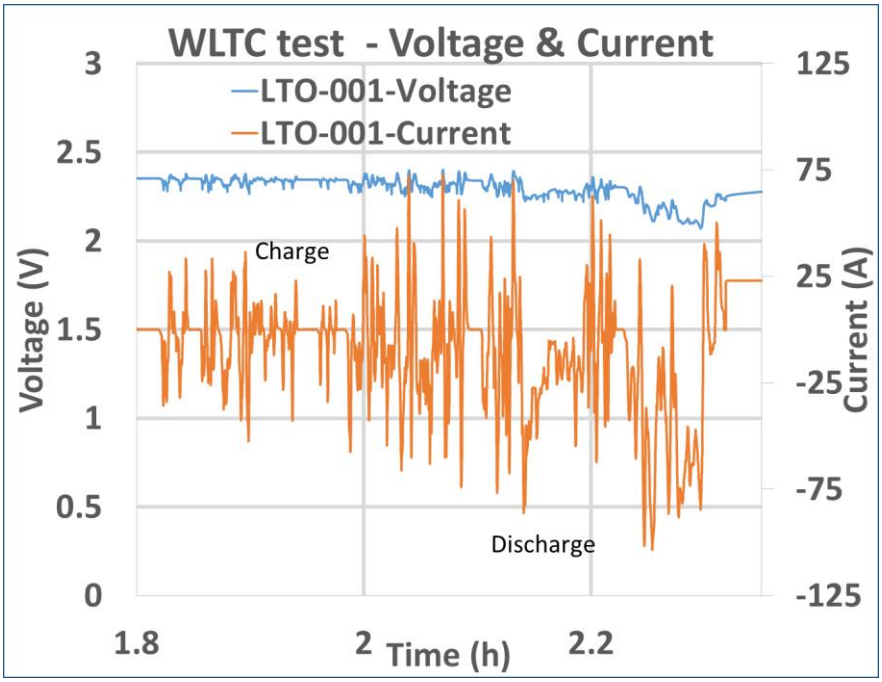

Figure 16. WLTC profile as a function of temperature.

3.2 Results from standard data collection for thermal modeling

3.2.1 Temperature measurement

For every test, a maximal allowable temperature is defined to prevent gassing and critical failure of the cell resulting from overheating and thermal runaway. Also, the evolution of the temperature is an important parameter for designing a thermal model. Thus, it is necessary to have a reliable way of measuring battery temperature.

Because only one point of the battery can be measured for temperature, this point has to be carefully chosen. Heat source diffusion has already been made with the cells chosen in this study.

To obtain the most suitable spot for placing the thermocouple, high-current discharge test at maximum discharging c-rate, 184A (8C) was performed and recorded by using infrared (IR) imaging. In this context, the experimental result of the cell's surface temperature distribution at 25°C was obtained and it is displayed in Figure 17 for different time intervals.

From this figure, it can be reported that the point of high interest is located near the negative tab. Therefore the k-type thermocouple will be placed on this spot during the thermal characterization.

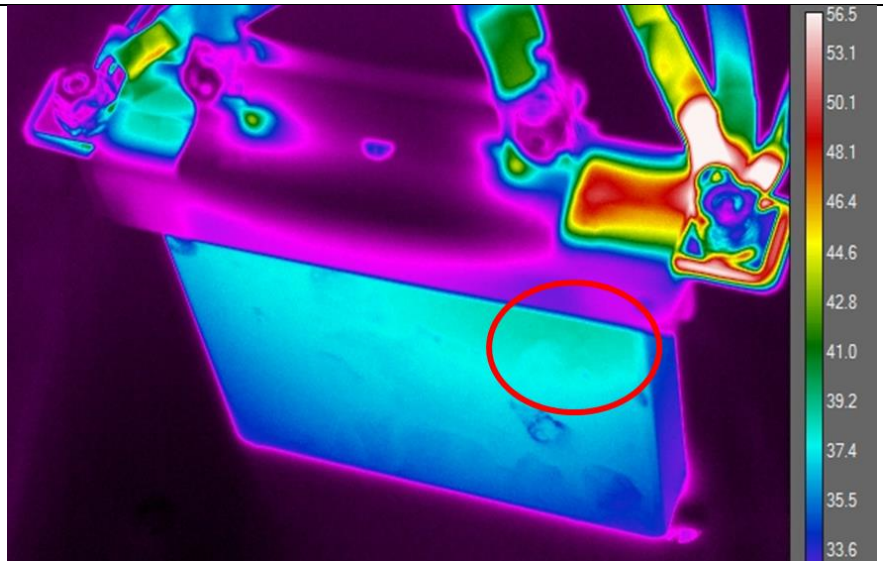

Time = 100s

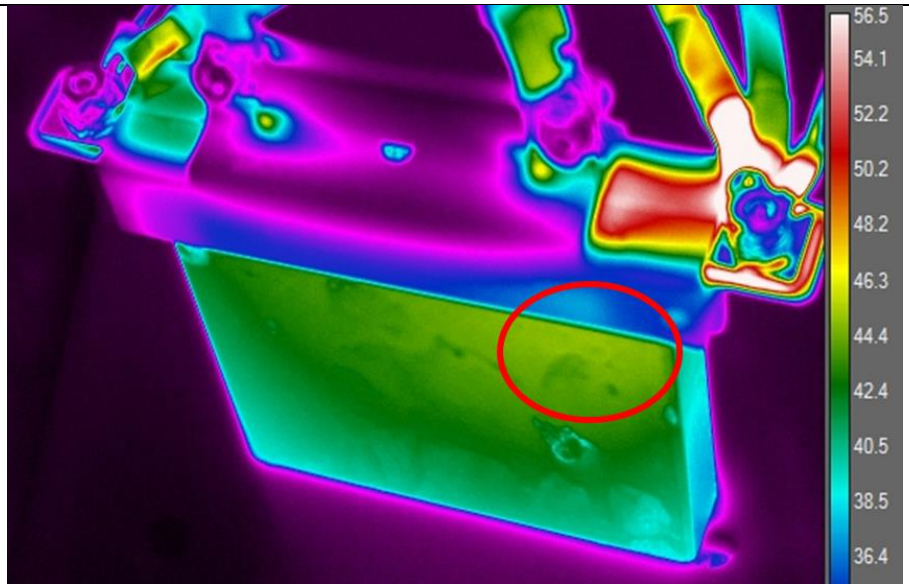

Time = 250s

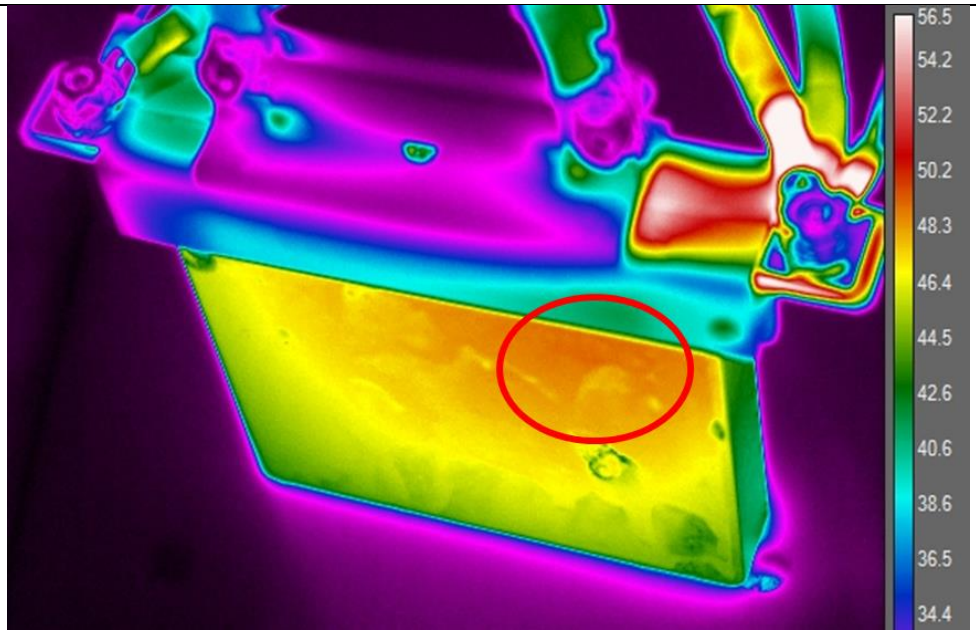

Figure 17. Temperature point of interest for the LTO cell at different time intervals.

3.2.2 Results for the specific heat capacity test

One usual manner to determine the C_p is to use calorimetry. However, such equipment is quite expensive especially when the tested cell presents quite a volume like for prismatic-shape cells. In this project, we propose a method to assess this parameter without the use of any calorimeter. The method used to assess the specific heat capacity involves high current rate in order to reach the thermal steady state of the system for which the generated heat is equal to heat losses by the system

As shown as in Figure 18, the profile used in this paper to assess the specific heat capacity (*Cp*) involves charging and discharging pulses at the manufacturer's recommended maximum rates. The profile is called a micro-pulse and is conducted at a fixed SOC of 50%. The first goal of this profile is to extract and inject the same number of Ah to the cell, in order to not have a dependency of the SOC, which can influence electrical and thermal parameters such as the cell resistances. The second aim to this profile is to reach rapidly a constant temperature at which the cell starts to lose the same amount of heat it is gaining (steady state), where thermal parameters such as convective heat transfer can be obtained. As for the C_p, the period, for which the surface temperature is increasing (transient state), is considered for comparison with the model. Then, the test profile is repeated at different temperatures to obtain the parameters' behaviors against thermal gradient.

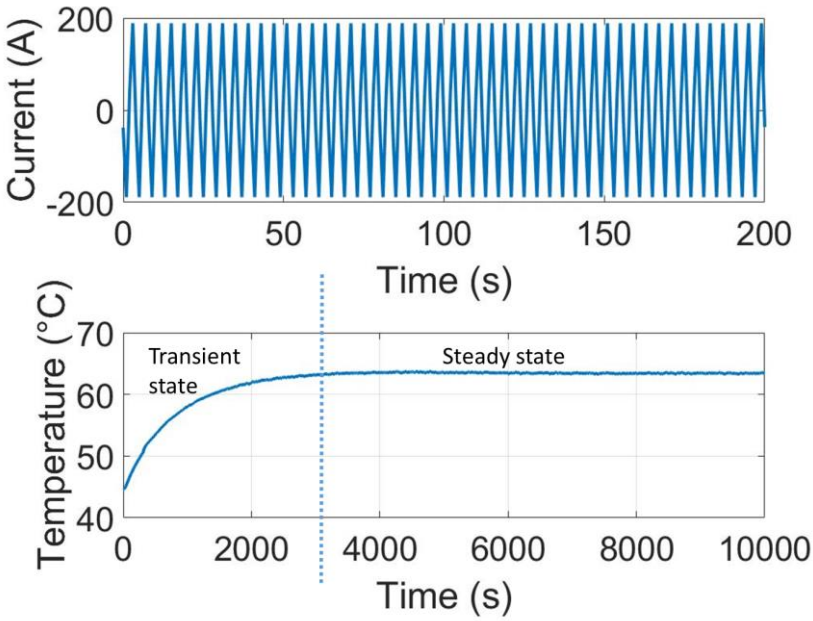

Figure 18. Micro-pulse test at 25°C.

3.2.3 Results from the OCV thermal test capacity test

In Figure 19, the applied cycle is shown and consists of the following: within 6 h the cell is kept at a certain SOC and the ambient air temperature is reduced to −25 °C ± 2 °C and is kept at this value for 6 h. Within the next 6 h, the temperature is increased to +23 °C ± 2 °C. Five test cycles are performed. In the same figure, the result of the OCV variation with temperature can be observed for different SOC points of the LTO cell: 90% and 70%. As can be seen, the temperature does not have a significant influence on the OCV values.

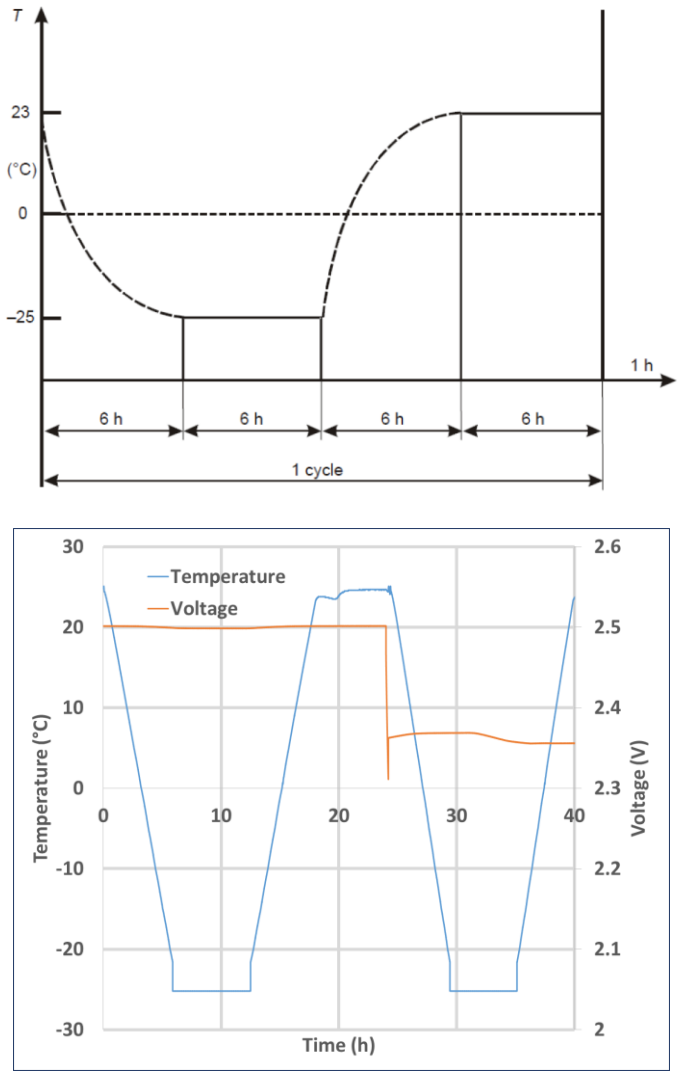

Figure 19. OCV thermal test, profile, and results.

3.2.4 Thermal validation tests

In order to correctly validate the electro-thermal model created based on the parameters acquired from the different characterization tests, two independent types of validation tests are additionally performed: the constant current and dynamic current test. These tests can be used to compare the output of the model with the temperature response of the cell.

3.3 Conclusion on the characterization

In this report, a detailed understanding of the electro-thermal behavior of LTO 23 Ah batteries has been proposed. VUB characterization techniques in electric-thermal characterization have allowed in creating a good set of electrical and thermal parameters which can be implemented to perform electric and thermal model activities. The results of the electric-thermal characterization tests highly influence the outcome of the battery model. The type of tests is always the same but the difference comes in by way of careful implementation of the test itself, battery connections and intricate modifications in the test protocols. Such dedicated modifications have led to the creation of a qualitative set of electro-thermal characterization tests at different C-rates, SOC levels, and temperatures.

The results of the characterization test of the LTO chemistry of the GHOST project were as expected and matches with the general information provided by the manufacturer data sheet. In the coming section, the validation of these parameters will be presented in a modeling study for which a 1D-electro-thermal model is developed.

4 Electro-thermal modeling of LTO cells

In this section, it is demonstrated how the cell electro-thermal parameters obtained in the previous from experimental work can be used to effectively model the voltage behaviour and the surface temperature of the cells under various scenarios. Modelling the cell temperature during operation is often required to ensure the cell is kept within the required temperature limits and also to calculate the cooling power required for thermal management application. A full presentation of the model is presented in Annex B.

4.1 Description of the used methodology

In this study, a 1D-electro-thermal model is used. The model is based on the semi-empirical approach in a MATLAB/Simulink® interface. The aim of the model is to reproduce the cell's electrical and thermal performances with two parts: the electrical and thermal parts, as shown in Figure 20. The first part deals with voltage response calculation with the electrical parameters. The second one estimates the cell temperature based on the heat generation equation. This methodology for the lithium-ion cell thermal model has repeatedly used in the literature with success and will be therefore adopted.

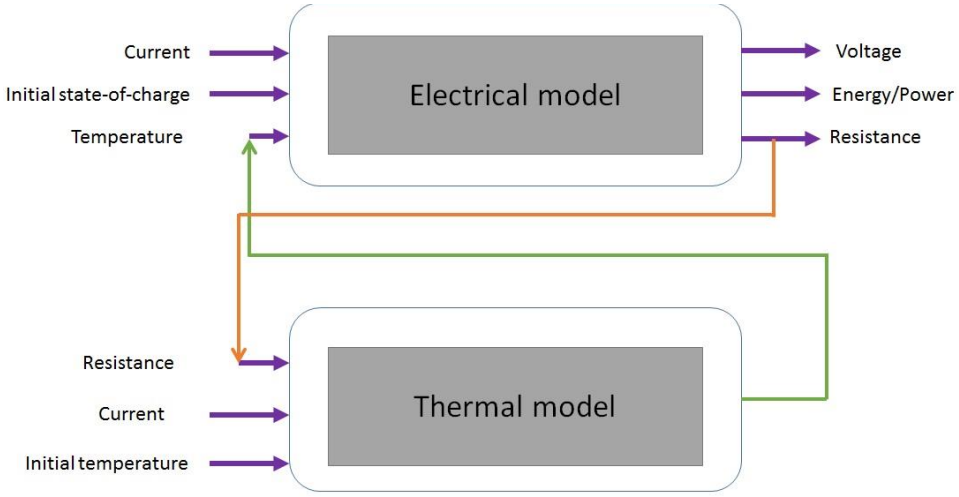

Figure 20. Schematic of the modelling methodology.

4.2 Development of the electrical model

4.2.1 Description of the electrical model

The electrical model is built on the Thevenin model [5] (See Figure 21) and consists of a voltage source with an ohmic resistance and a parallel RC circuit. Based on the equivalent circuit model, the battery output voltage of the Li-ion cell is the voltage drop resulting from the battery open circuit voltage (OCV), the battery ohmic resistance (R_0), and battery polarization impedance (R_1C_1 circuit). The output voltage of the cell is then calculated by [5]:

$$V_{cell} = V_{oc} - R_1 I_1 - R_2 I_2 - R_0 I_{batt} \qquad (1)$$

where Ibatt is the flowing current in the battery (A), I_1 is the current passing in the polarization resistance (A) and I_2 is the current flowing through the charge transfer one (A). Next, the level of charge or SOC is determined by the coulomb-counting method and is defined as [6]:

$$SOC = SOC_0 - \frac{1}{C_{init}} \int I_{batt} dt \qquad (2)$$

with SOC_0 the initial state-of-charge of the cell. C_{init} is defined as the initial capacity (Ah) and it is assumed to depend on temperature [7] and current:

$$C_{init} = f(T, I) \qquad (3)$$

In equation (1), all the circuit parameters are defined through lookup tables with V_{oc} pulse tests that correspond to a specific SOC and temperature [8]. The pulses were performed at a 10%-step of SOC from 100% to 0% at four temperatures. Then, an estimation fitting algorithm in Matlab/Simulink was used to fit the simulation and experimental data and extract each parameter point. Based on these parameters the heat generation is calculated in the thermal part of the model.

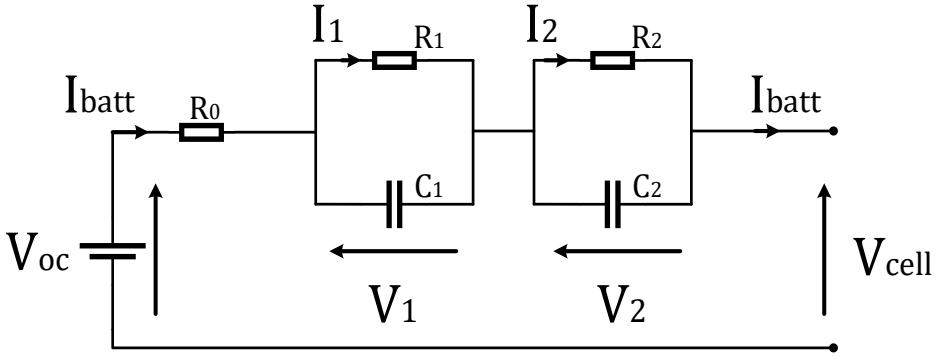

Figure 21: representation of the 2nd-order Thévenin model.

4.2.2 Results of the characterization for electrical modeling

As explained before, the Dual Polarization (DP) equivalent circuit model is employed to describe the GEIRI cell's behavior. It is illustrated in the where R_0 is the ohmic resistance, Vocv is the open circuit voltage, VL is the voltage at the battery terminals and the 2 parallel RC branches represent the concentration and activation polarization (or charge transfer resistance) resistance $R_{p1}//C_{p1}$ and $R_{p2}//C_{p2}$ respectively. Figure 24 to Figure 28 show the electrical parameters for the 2nd order model (see next section) extracted from the HPPC test for one cell, tested at 25 degrees. The figures show the resistances and time constant for the cell as a function of SOC and current rates separately for charge and discharge pulses.

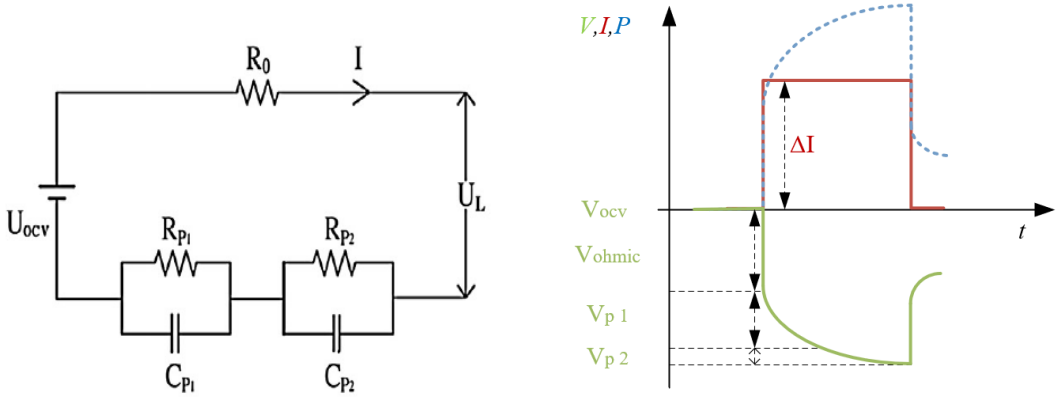

Figure 22. The corresponding region of the pulse and the schematic of the electrical model.

The corresponding region of these electrochemical reactions during a current pulse is also shown in Figure 22. The model is characterized by extracting the electrical components values based on the equations describing the DP ECM as shown below:

The DP model

$$\begin{cases} U_L = U_{ocv} - IR_0 - U_{p1} - U_{p2} \\ \dot{U}_{P1} = -\dfrac{1}{C_{P1}R_{P1}}U_{P1} + \dfrac{1}{C_{P1}}I \\ \dot{U}_{P2} = -\dfrac{1}{C_{P2}R_{P2}}U_{P2} + \dfrac{1}{C_{P2}}I \end{cases} \quad (4)$$

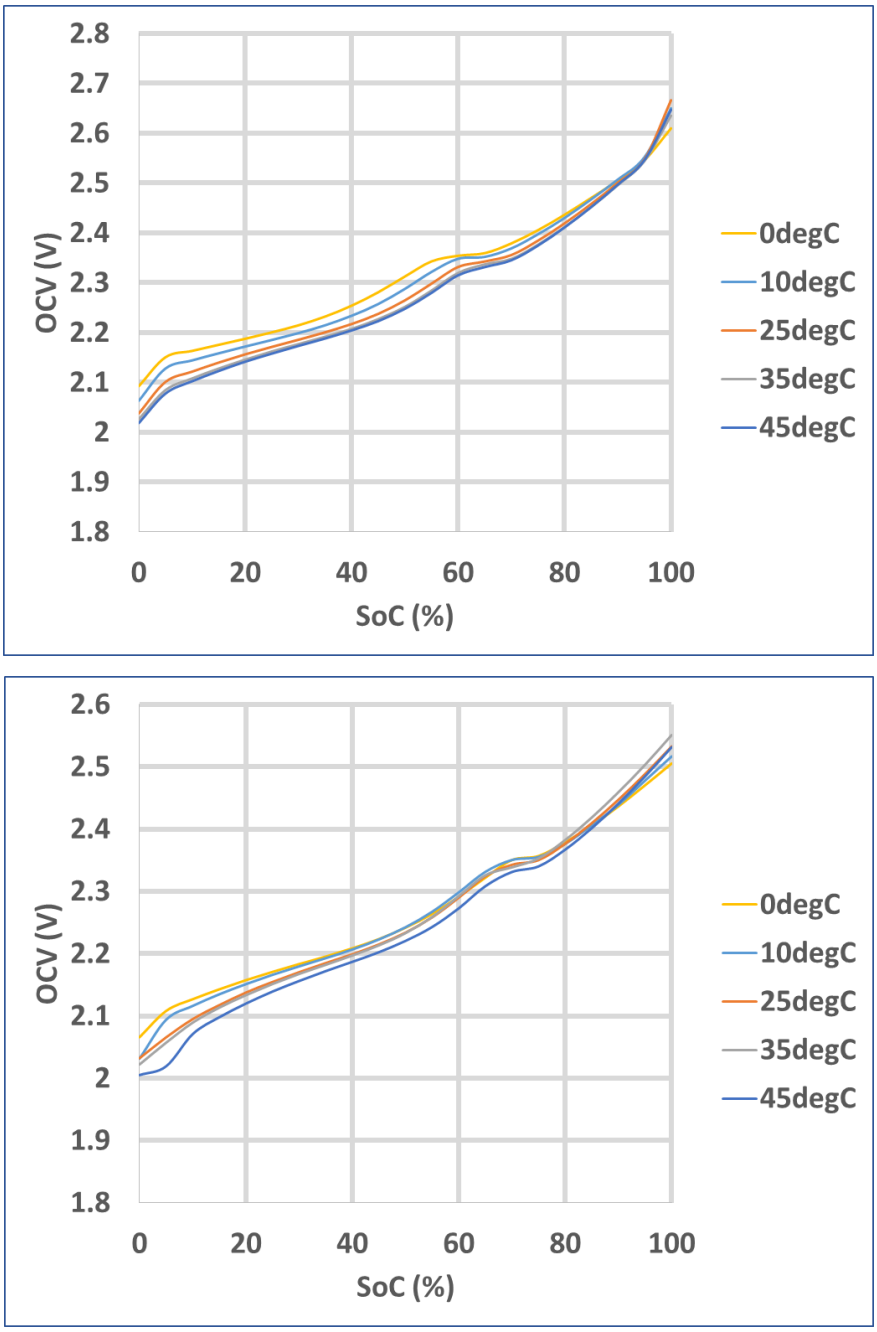

Figure 23. Discharge (top) and charge (bottom) OCV as a function of temperature and state of charge.

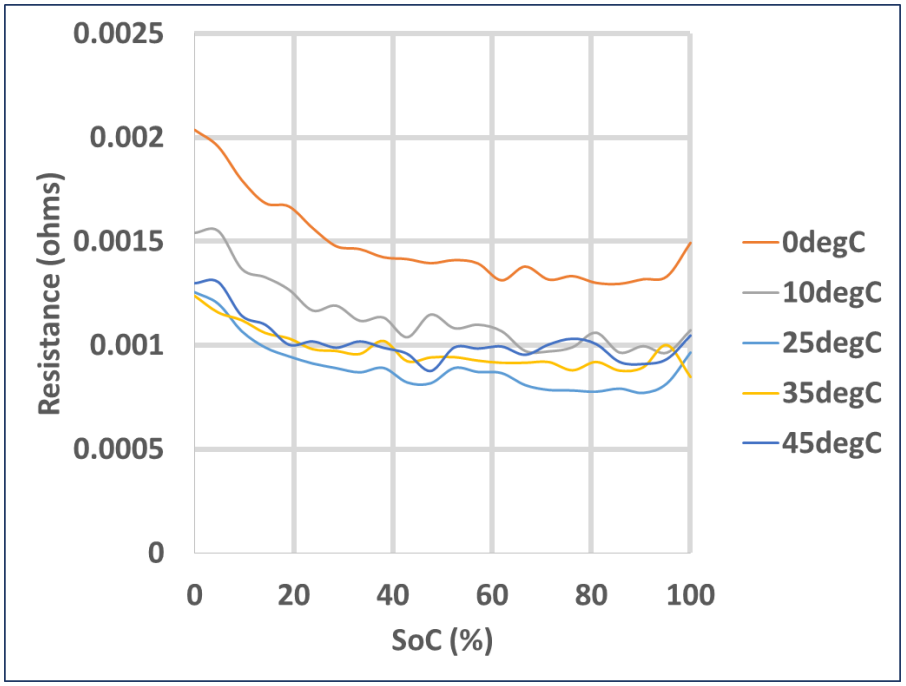

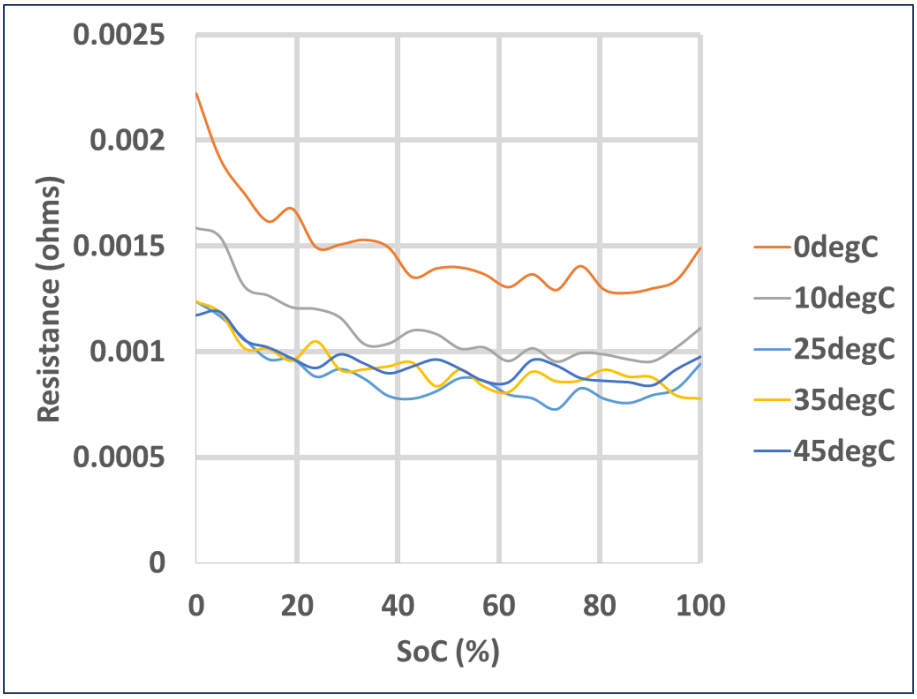

Figure 24. Ohmic resistance as a function of temperature and state of charge for the discharging (top) and charging states (bottom).

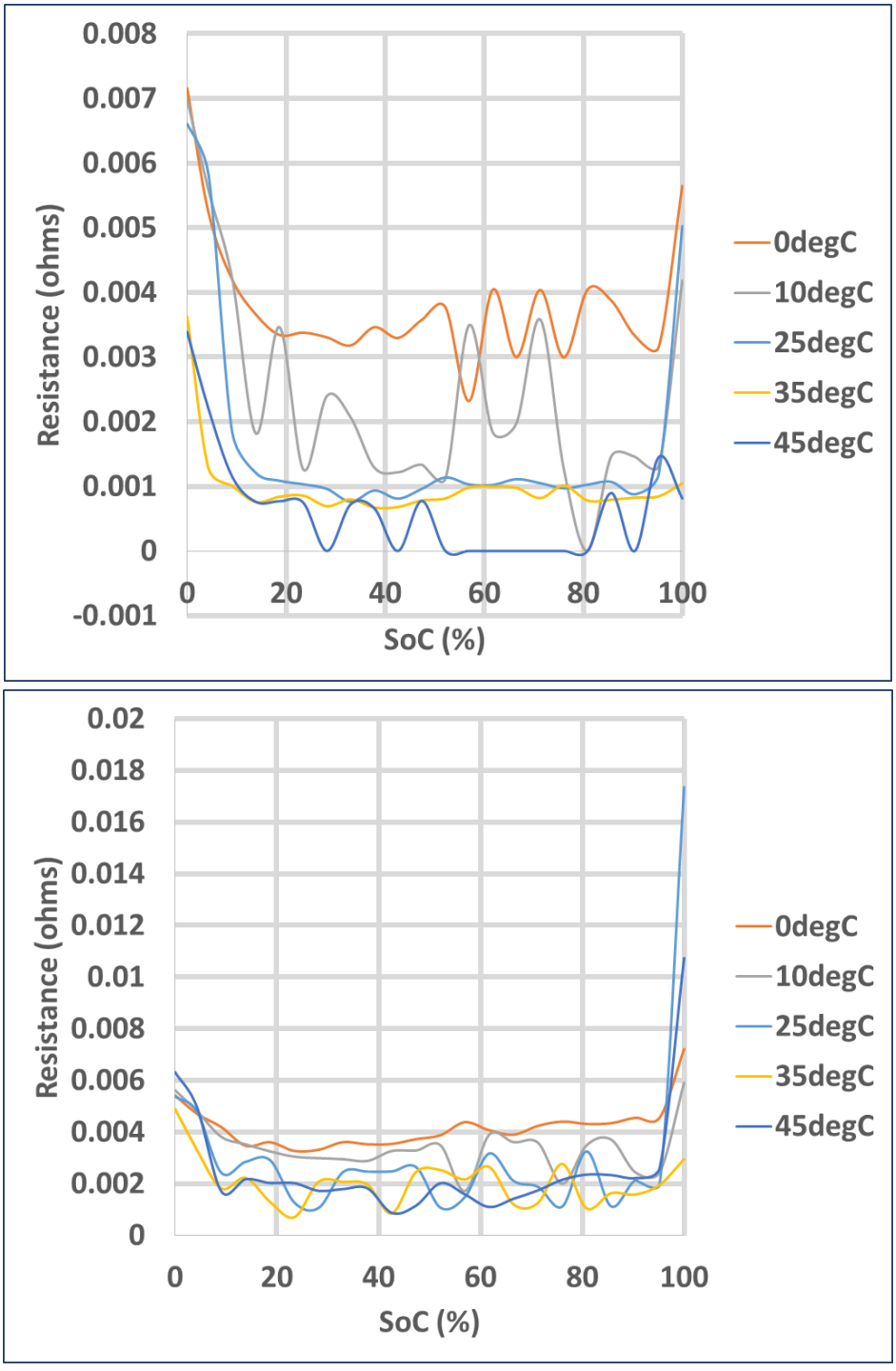

Figure 25. Polarization resistance as a function of temperature and state of charge for the discharging (top) and charging states (bottom).

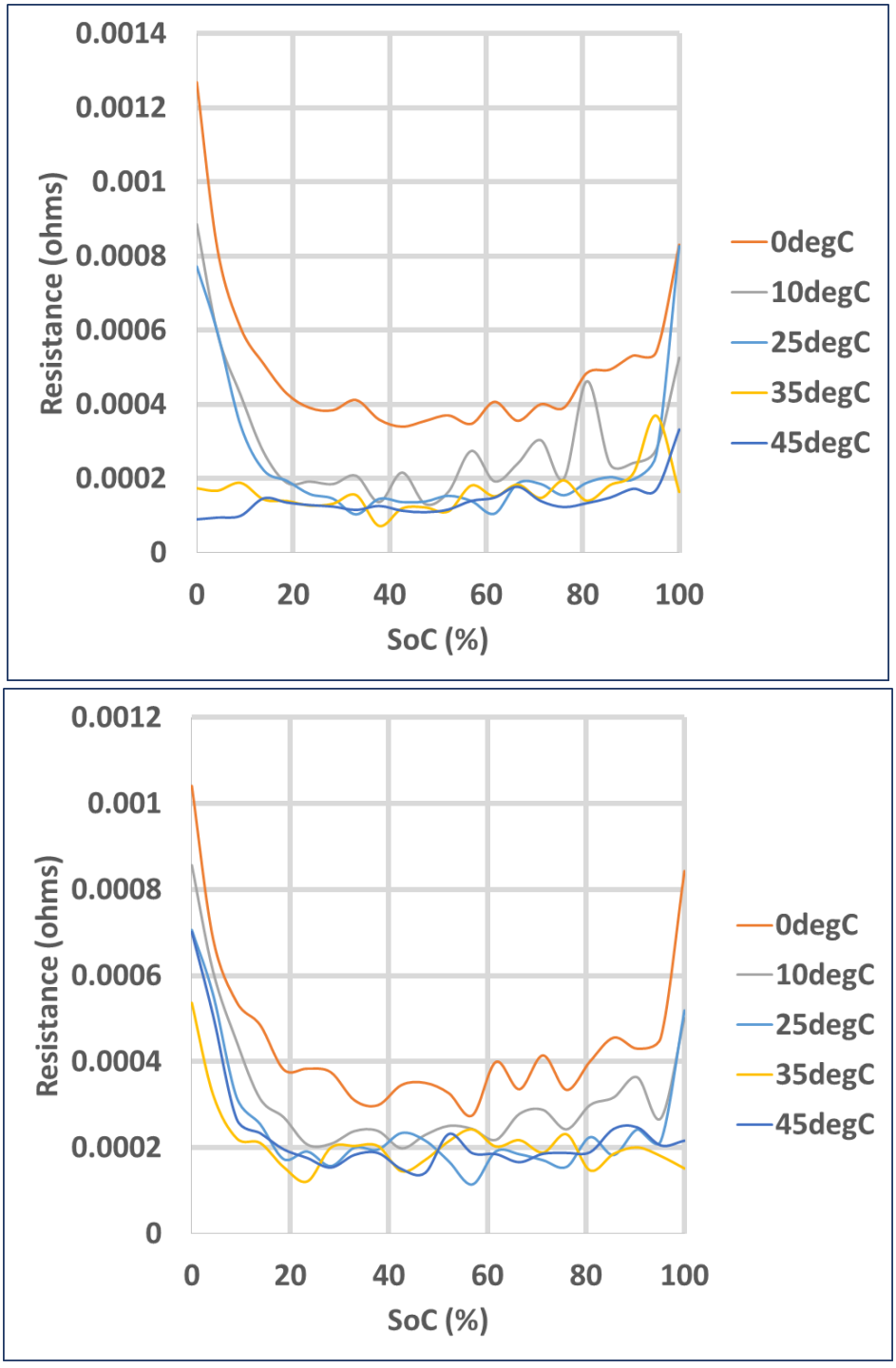

Figure 26. Polarization resistance 2 as a function of current rate and state of charge

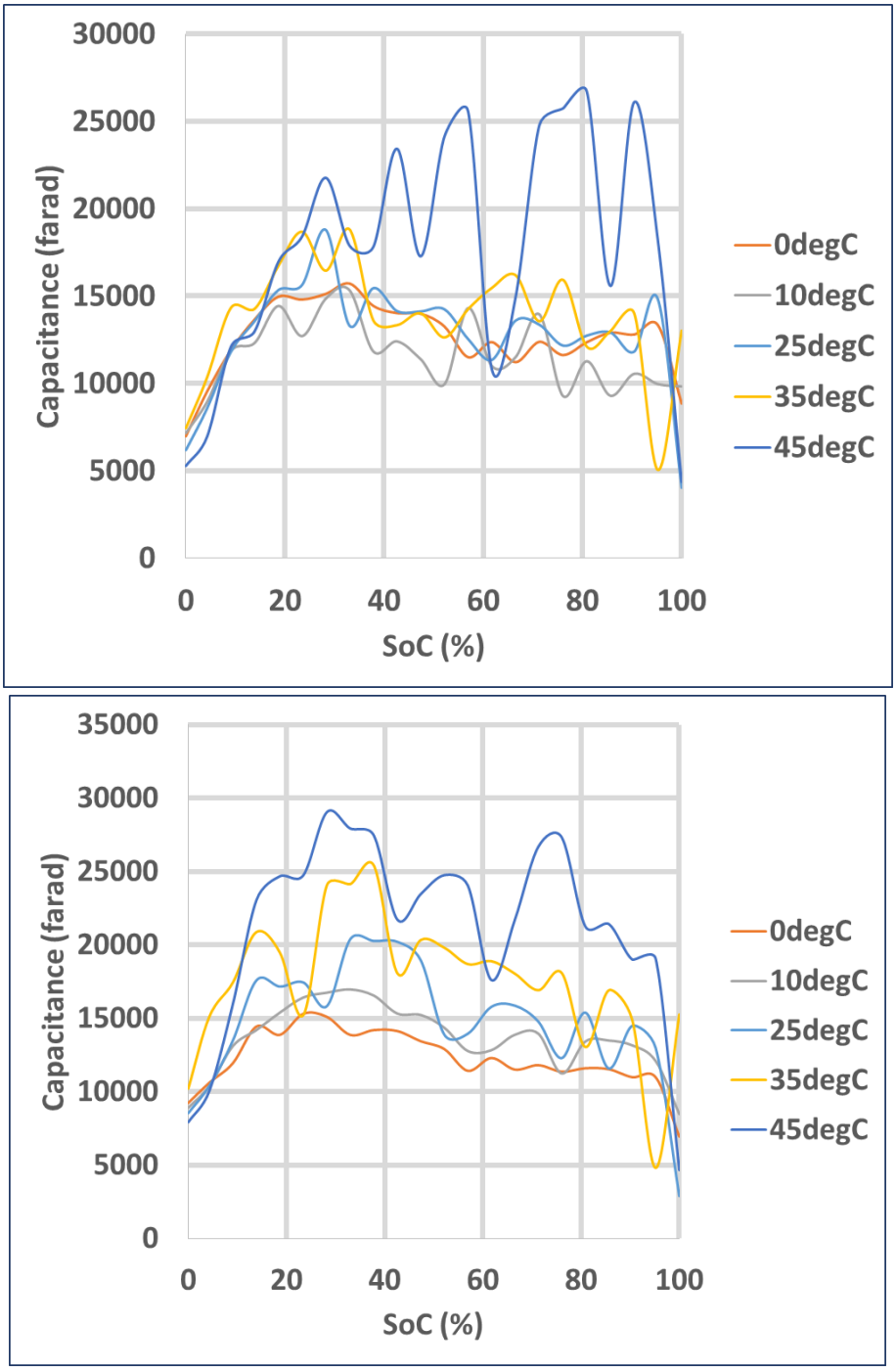

Figure 27. Time-constant as a function of current rate and state of charge

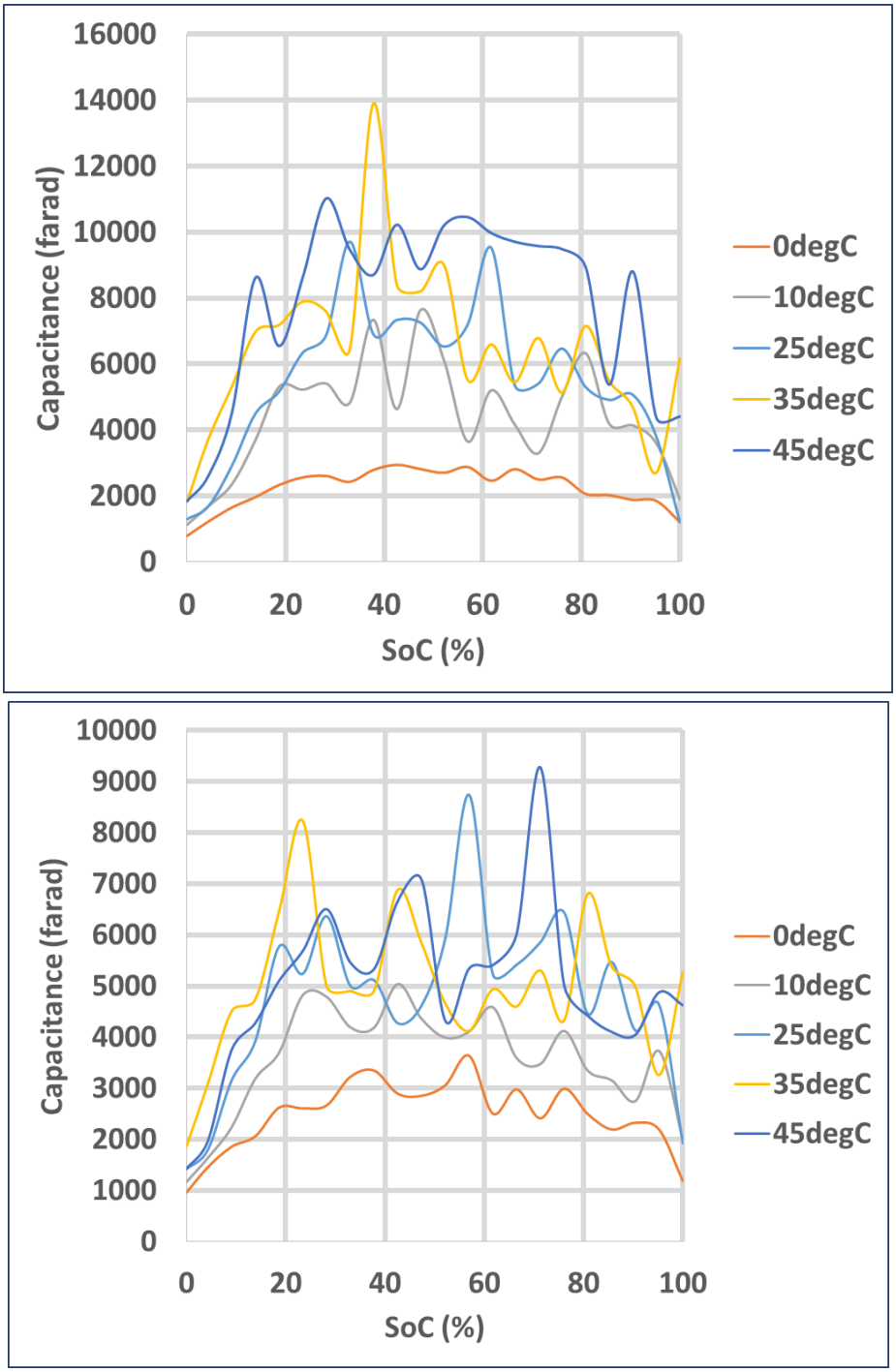

Figure 28. Time-constant 2 as a function of current rate and state of charge

The parameters are extracted and collected into organized lookup tables which are a function of the state of charge, cell temperature and C-rate. As an example, the look-up table of R_0 is shown in Annex A, Table 15.

4.2.3 Results of the validation for electrical modeling

In order to correctly validate the electro-thermal parameters, some independent validation tests were performed accordingly to the validation profiles explain in the last section. Regarding the electrical part, the validation test consisted of applying a dynamic profile from 90% to 10 SOC to represent the electrical input of a BEV. The results of the validation for which the measured and estimated voltage for the cell under the loading condition at five temperatures: 0°C, 10°C, 25°C, 35°C and 45°C are shown from Figure 29 to Figure 33. It is clear from the figures that the modeled voltage closely matches that of the voltage obtained during the electrical experiments hence providing further evidence of the authors' electrical modeling and the estimated electrical parameters. The error is calculated with the root-mean-square error (RMSE) for which the RMSE of simulation results are the deviation from the measurement data reflects the efficiency of the model for the capacity tests. Table 14 lists the model deviation for which an average of 2% error is depicted hence emphasizes the good modeling technique used in this report.

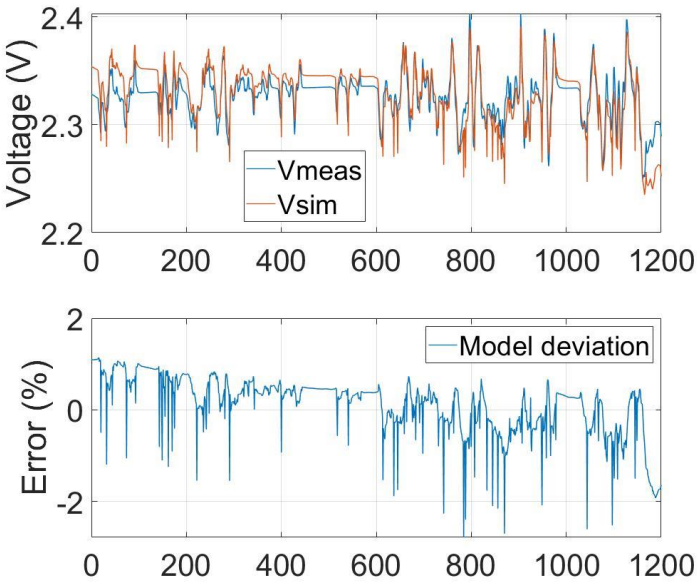

Figure 29. Validation of the NMC electrical model at 25°C.

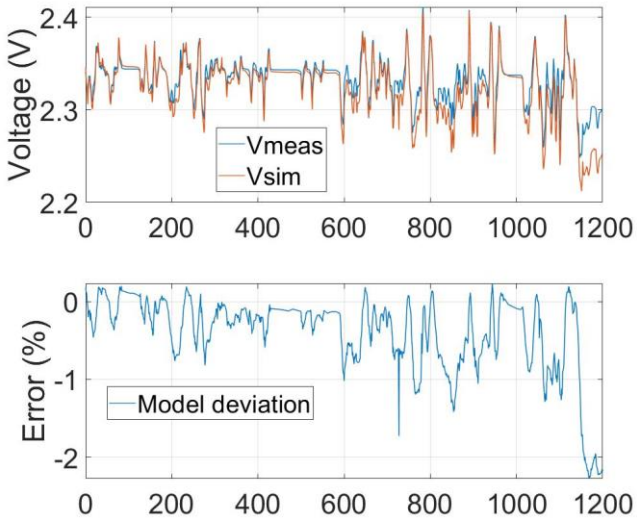

Figure 30. Validation of the NMC electrical model at 35°C.

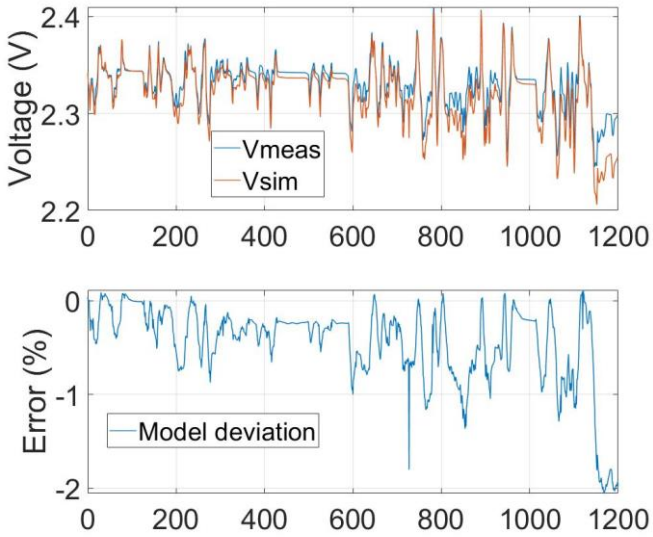

Figure 31. Validation of the NMC electrical model at 45°C.

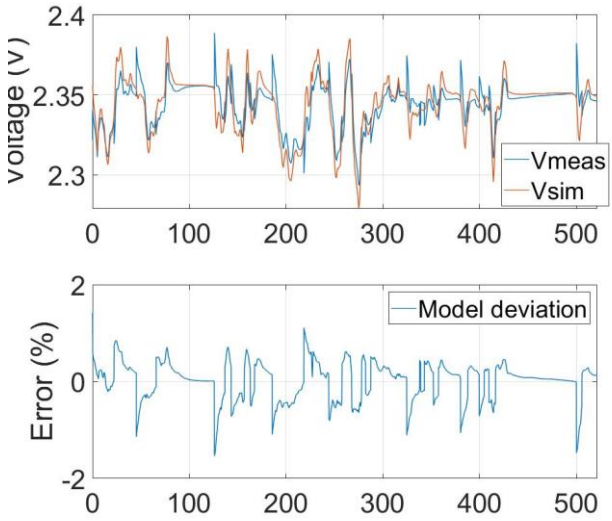

Figure 32. Validation of the NMC electrical model at 10°C.

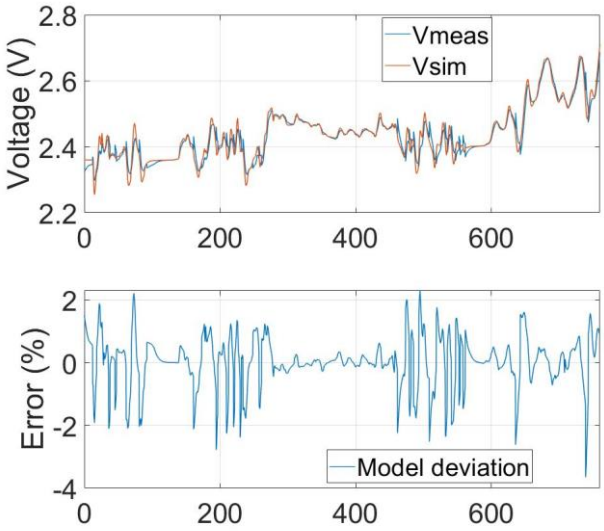

Figure 33. Validation of the NMC electrical model at 0°C.

Table 14. Electrical model deviation.

LTO electrical model deviation					
Temperature (°C)	0	10	25	35	45
Mean RMSE (%)	2	2	2	1	1

4.3 Development of the 1D-thermal model

4.3.1 Description of the 1D-thermal model

The thermal part of the model treats with the thermodynamics equations for prismatic-shape cells. In this part, as shown in Figure 34, heat is generated in a point located at the surface of the cell for which a specific heat capacity and a mass are found. The heat is then transferred from the surface of the cell to the ambient environment.

Conducting a heat balance equation at the point on the surface, the next equations obtained from thermodynamics [9], solve the heat transfer between the surface and the ambient:

$$\left\{\begin{array}{c} \frac{dU_{cell}}{dt} = Q_{gen}\,(t) - Q_{loss}\,(t) = m.Cp.\frac{dT}{dt} \\ Q_{gen} = R_0.(I_{batt})^2 + R_1.(I_1)^2 + R_2.(I_2)^2 \\ Q_{loss} = Q_{conv} = h_{conv}S_{area}(T_{cell} - T_{amb}) \end{array}\right\} \quad (5)$$

where U_{cell}, the internal energy, is the total energy contained by a thermodynamic system (J), Q_{gen} is the generating heating rate (W) in the corresponding element, and Q_{loss} is the heat losses of the corresponding element (W). C_p is the specific heat of the cell (kJ/kg.K) and m is the mass of the cell (kg).

The following assumptions are made for the thermal model:

- The temperature of the surface of the cell, Ts is assumed to be uniform and therefore it represents the temperature of the whole cell.
- In this paper, heat generation is characterized only by ohmic losses, because the largest heat source in the battery operation comes from the ohmic resistance [41].
- In the steady state of thermodynamics, resulting from the temperature being constant, the amount of generated heat is the same as the heat losses, therefore equation 4 becomes:

$$\left\{\begin{array}{c} 0 = Q_{gen}\,(t) - Q_{loss}\,(t) \\ Q_{gen} = R_0.(I_{batt})^2 + R_1.(I_1)^2 + R_2.(I_2)^2 \\ Q_{loss} = Q_{conv} = h_{conv}S_{area}(T_s - T_{amb}) \end{array}\right\} (6)$$

Natural convective heat transfer is considered in this paper with the following definition: T_{amb}, the area of heat exchange, S_{area} (m²), and the convective heat transfer coefficient h_{conv} (W/m².K). In this context, regarding the boundary limits of the model, the heat transfer with the surroundings is determined by following the convection equation

$$Q_{loss} = S_{area}.h_{conv}.(T - T_{amb}) \quad (7)$$

with A the exposed area (m²) and h the convection transfer coefficient (W/(m².K))

There are therefore two unknowns in Equation (5), C_p the heat capacity and h_{conv} the convective heat transfer coefficient. In this context, these two parameters are being determined based on a parameter estimation methodology described in the next section.

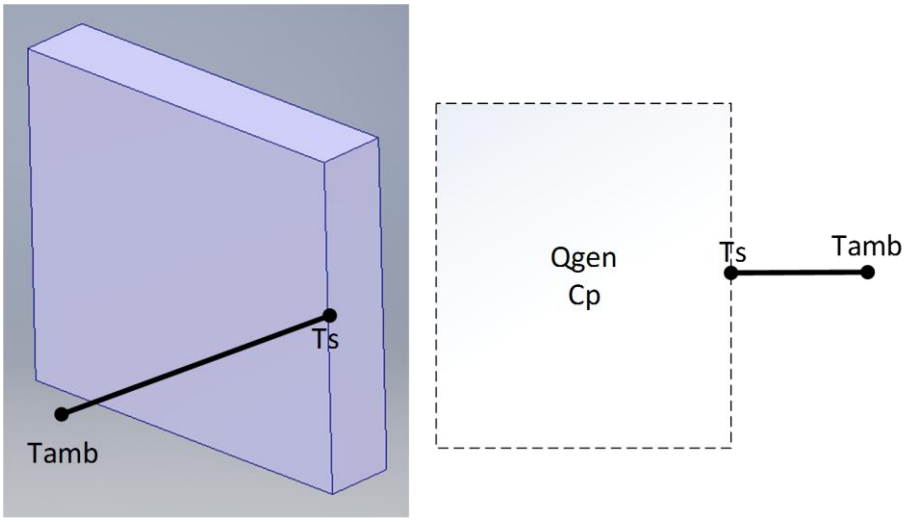

Figure 34: Overview of the thermal model with a 3D representation of a prismatic cell.

4.3.2 Results of the characterization for thermal modeling

The specific heat capacity (C_p) and convective heat transfer coefficient (h) of the cells are important for the thermal model. To obtain them, a fitting technique using a fitting model and a specific test is used. The dedicated test has been described in section 3.2.

To obtain the convective heat transfer coefficient, equation (6) is used in the steady state. For Q_{gen}, the average value of the heat generation of the test after 20 min is used. The heat generation is calculated with the electrical model described before and is 20.5 W for an 8C-micropulse test. The ambient temperature is fixed to the tested temperature (0°C, 10°C, 25°C, 35°C and 45°C)), as for the final battery temperature, is it extracted from the experimental results as the final temperature point after 20 min of the test.

Nonetheless, since it is difficult to estimate as it depends on many parameters and variables, the value of this coefficient changes constantly especially in a non-adiabatic chamber, therefore the coefficient gradient will not be reported in this report.

For the C_p, the same experiment as above is used but in the transient state where the temperature of the cell presents a clear evolution. The least squares regression of equation (5) is used to fit the surface temperature in a fitting model with the pre-defined value of h. The least squares regression described above is also repeated at other temperatures to find the thermal gradient behavior. The specific heat capacities obtained with the method explained above are graphed in Figure 36. From this figure, one can see that there is a weak positive correlation of the cell-specific heat capacity for the LTO cell with its temperature. Over the full temperature range subjected to the cell core, the average value of the specific heat capacity is 1150 kJ/(kg.K) for 50% of SOC.

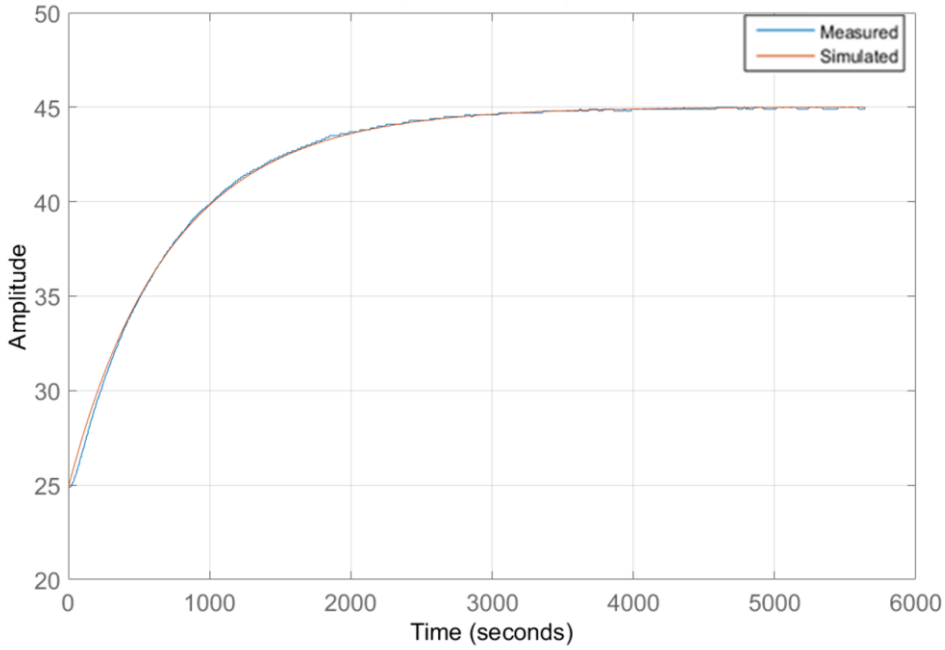

Figure 35. The fitting example at 25°C where the fitted temperature curve has been created using Equation (5).

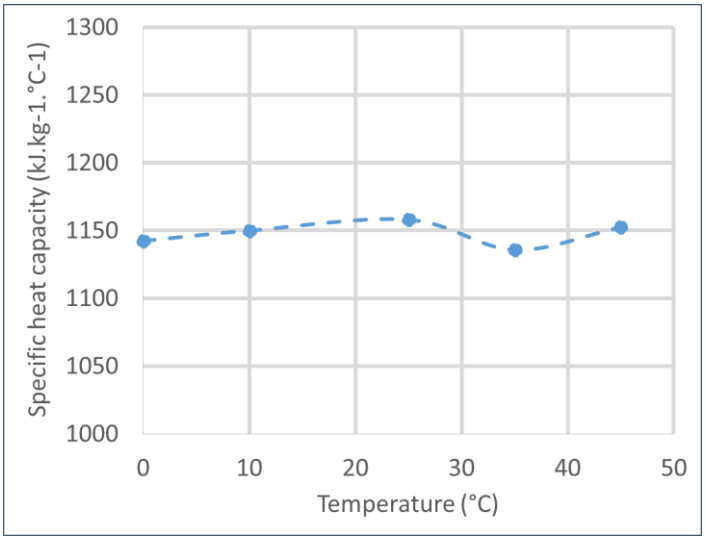

Figure 36. LTO specific heat capacities at different temperatures and at 50% of SOC.

4.3.3 Results of the validation for thermal modeling

And, for the thermal model, the validation test consisted of discharging the cell with a high constant current of 8C (184A) from 100% to 0% of SOC and at five initial temperatures (0°C, 10°C, 25°C, 35°C and 45°C). The results of these validation tests are shown in Figure 37 for which the variation of temperature, called ΔT, is displayed in order to compare the 4 tests. ΔT is a way of expressing temperature differences when conducting temperature tests and is calculated by subtracting the current battery temperature with the initial battery temperature. That is to say, it is a good way to compare different temperature test for which the initial temperature is not the same.

One can see that the ΔT is lower at high temperatures (45°C), the reason is that the resistance of the cell becomes lower in the high-temperature environment due to more active side reactions which translates a lower heat generation since it is based mainly on the Joules effect.

All graphs in Figure 38 have been realized using the values for C_p given in the last section and simulated using the model described in chapter 3. It can be observed that though only ohmic heat generation is treated, the model accurately predicts the surface temperature.

As a result, the good model agreements of the electrical and thermal behaviors with experimental results also underline the validity of the model. Moreover, this validation provides robust evidence of the authors' heat capacity assessment as well the 2^{nd} Order Thevenin model discussed earlier.

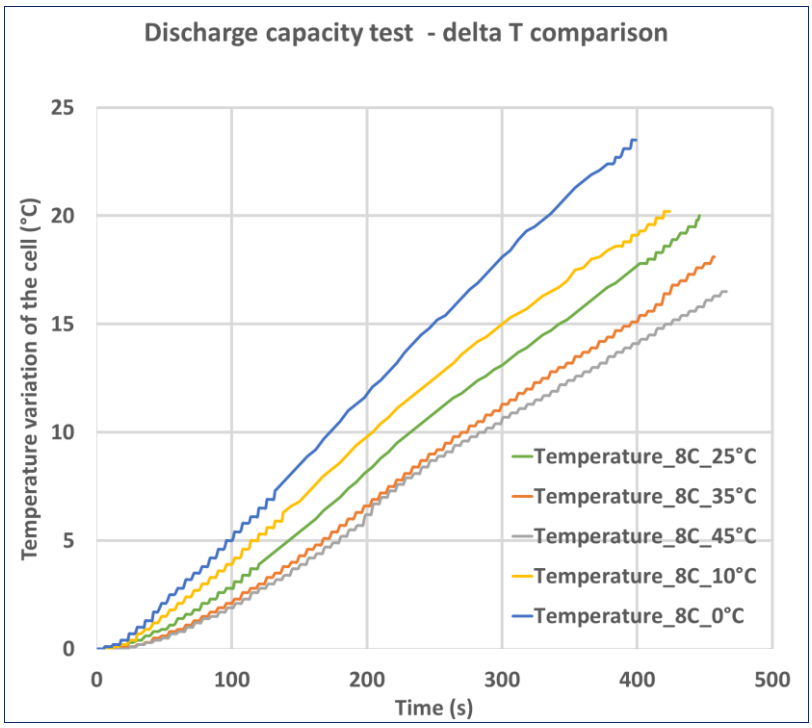

Figure 37. Temperature variation at 8C for a constant discharge test.

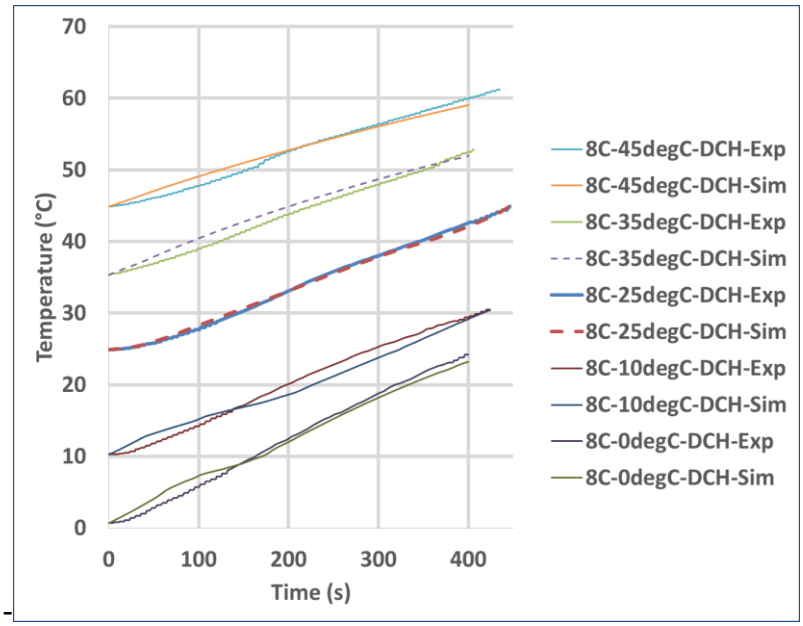

Figure 38. Validation of the LTO thermal model at different initial temperatures.

4.4 Development of the 3D-thermal model

4.4.1 Description of the used methodology

As shown in Figure 39, a 3D-thermal model of a lithium-ion cell is built, which treats the battery as a core with two tabs. It is an effective method to couple a 1D electrochemical with a 3D thermal model to study cell's temperature and voltage characteristics [1], [2] However, as it was reported in [3], lots of parameters are required to operate the electrochemical model, and some of them require invasive and expensive techniques to be obtained, such as the length of the electrode or the diffusivity coefficient. In addition, a thermal behavior model is essentially an energy conservation equation in each representative elemental volume of the cell at any given time interval, i.e., the sum of the absorbed and generated heat equals the sum of the lost heat and the increased internal energy inside the micro-unit. Therefore, a key requirement for the accuracy of a 3D thermal modeling is to obtain the generated heat flowing inside the prismatic cell.

An electrical model based on the ECM approach is used instead of an electrochemical model to assess the heat generation estimation. The electrical model development was described in the previous section and we invite the readers to review this report in case of questions.

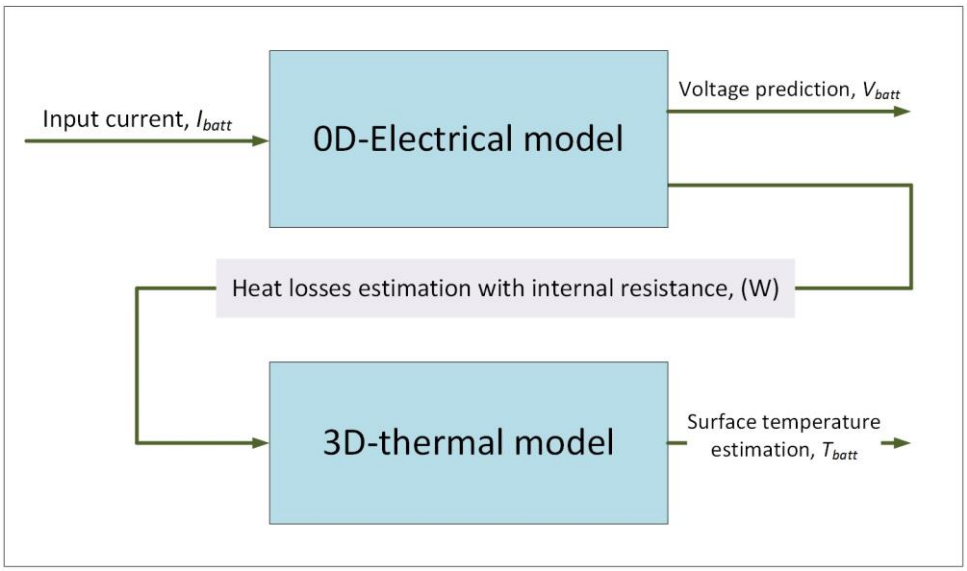

Figure 39. Schematic of the couple 1D / 3D modeling methodology.

4.4.2 Description of the 3D-thermal model

In this section, a 3D-thermal model is developed to investigate the thermal behaviour of the LTO at different environmental conditions. The energy balance equation over the computational domain is as follow:

$$\rho C_p \frac{\partial T}{\partial t} + q_v = k_x \frac{\partial^2 T}{\partial x^2} + k_y \frac{\partial^2 T}{\partial y^2} + k_z \frac{\partial^2 T}{\partial z^2} \quad (8)$$

where ρ, C_p, k are density(kg/m^3), specific heat capacity(J/(kg.K)) and thermal conductivity(W/m.K), respectively. The thermal conductivities are anisotropic in the 3D thermal model. Generally, it has a greater value along with the battery sheets than in the direction normal to the sheets. Usually, the thermal conductivity in x,y and z-axis are calculated from the formula as follow:

$$k_{T,y} = \frac{\sum L_{i,y}}{\sum \frac{L_{i,y}}{K_{T,i,y}}} \quad (9)$$

$$k_{T,x} = \frac{\sum L_{i,x} K_{T,i}}{\sum L_{i,x}} \quad (10)$$

$$k_{T,z} = \frac{\sum L_{i,z} K_{T,i}}{\sum L_{i,z}} \quad (11)$$

Nonetheless, in order to calculate theses conductivities, the exact composition of the materials composing the cell should be known. Invasive testing is required to obtain these parameters. Fortunately, the manufacturer of the cell, Toshiba, has provided these values obtained from in-depth testing. The values of the conductivities are displayed in the next section.

The heat generation of the cell is then calculated from the resistance of the cell by equation 13 and for the tab domains, the heat generation is given by equation 14 as follows:

$$\frac{dU}{dt} = Q_{gen} - Q_{loss} = m.C_p.\frac{dT}{dt} \quad (12)$$

$$Q_{gen} = R_{th}.I^2 \quad (13)$$

$$q_{tab} = \frac{R".I^2}{V_{tab}}; \quad R" = \rho" \frac{l}{S} \quad (14)$$

with *m* the mass of the cell, dT the temperature difference intrinsic to the system and C_p the specific heat capacity of the cell (J/(kg.K)). The value of C_p is commonly found in the literature: 1200 kJ/(kg.K) and 1500 kJ/(kg.K) for LTO. In this study as it is mentioned in the 1D-thermal model, the value of C_p calculated 1150 kJ/(kg.K).

For the heat generation of the cell, Q_{gen} is heat generation (W) and *I* the battery current (A). For the tab domains R" (Ω), ρ" (Ωm), l (m), S (m^2) and V_{tab} (m^3) are the electrical resistance, resistivity, length, cross section and volume of the corresponding tab, respectively.

Finally, regarding the boundary limits of the model, the heat transfer with the surroundings is determined by following the convection equation

$$Q_{loss} = A.h.(T - T_{amb}) \qquad (15)$$

where, *h*, *A*, *T*, and T_{amb} represent the convection heat transfer coefficient(W/(m².K)), the surface area(m^2), the surface temperature(K), and the ambient temperature(K), respectively.

With the purpose of the simulation of the non-uniform temperature distribution through the cell domain, a computationally efficient localized heat source model has been implemented in the cell domain. Between the different techniques of measuring cell surface temperature, thermal infrared (IR) imaging is one of the best potential tools that can be used to detect and measure this spatially non-uniform temperature distribution with reasonably high precision. According to the IR image, at an ambient environmental condition shown in Figure 41, the cell is divivided intwo zone, one is a hot zone in the centre and on higher part of the battery and one cold in the lower. Therefore, in the model, the cell domain is divided into two domains. The hottest zone is specified by the dashed line in Figure 41 and the zones generally divided by the border between the hot and cold zone.

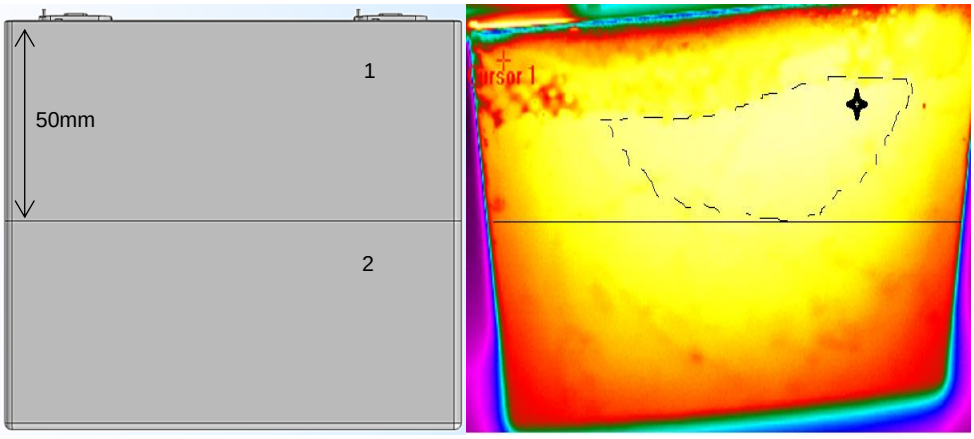

Figure 40. Different zones in the cell domain for the localized heat source model at 25°C.

The coefficients of *α* and *β* were calculated based on the surface temperature value. The temperature was measured experimentally by a thermocouple in the hottest zone.. Accordingly, we have used the same spot thermocouple on the surface of the cell in the CFD model and simulations.

The total heat generation in the cell for each zone is formulated as follows:

$$Q_{cell} = Q_1 + Q_2 = \alpha Q_{cell} + \beta Q_{cell} \quad (16)$$

$$\alpha + \beta = 100\%$$

$$Q_1 = \frac{\alpha Q_{cell}}{V_1}, \; Q_2 = \frac{\beta Q_{cell}}{V_2} \quad (17)$$

where the α, V_1, β , V_2 are the percentage of total heat generation and volume of upper and down zone respectively.

We defined a model deviation coefficientΔT_{error} (℃) in order to obtain the tuned values of α and β when comparing the thermal picture with the simulation. ΔT_{error} represents the temperature difference of IR image and simulation in specified hottest zone spot.

$$\Delta T_{error}(°C) = |T_{IR} - T_{sim}|$$

where T_{IR} is the surface temperature (°C) of the IR image and T_{sim} is the surface temperature (°C) of simulation. The amount of α and β is specified once the temperature difference or the model deviation becomes less than 2℃ .

4.4.3 Results of the characterisation for thermal modelling

In this report, according to the description of the model, the parametrization of the 3D-thermal model allows the variation of the heat generation rate with time, SOC, C-rate and temperature for it is calculated with the electrical model.

The other thermal parameters (conductivity, specific heat capacity) are determined through specific tests. For the Cp, the values obtained in the previous section for the thermal model will be used.

Regarding the conductivities, the values will be directly obtained from the manufacturer's datasheet.

4.4.4 Results of the validation for thermal modelling

For the thermal model, the validation tests consisted of discharging the cell with a high constant current of 8C (184A) from 100% to 0% of SOC and at five ambient temperatures (0°C, 10°C, 25°C, 35°C and 45°C). The results of these validation tests are shown in Figure 37. It is a good way to compare different temperature test for which the initial temperature is not the same. It is obviuos from the temperature profiles of Figure 42 for each ambient temperature, the temperature reaches its maximum at the end of the cycle. In this part, the pictures taken by IR image at the end of the test were compared with simulation results at five ambient temperatures (0°C, 10°C, 25°C, 35°C and 45°C). As a result, the good model agreements between numerical and experimental results underline the validity of the model.

Time(s)	Initial temperature (℃)	Thermal camera picture	Simulation
457	0	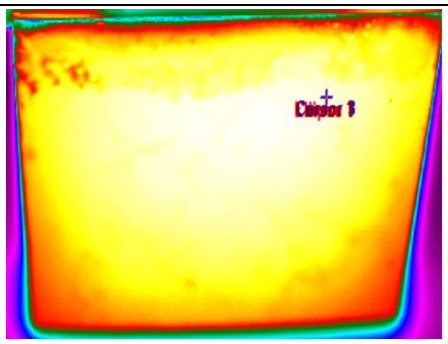	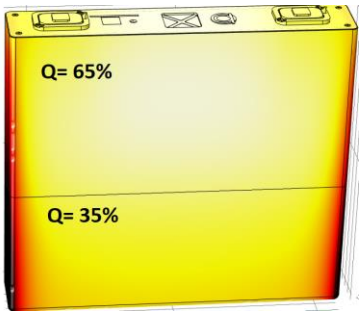
434	10	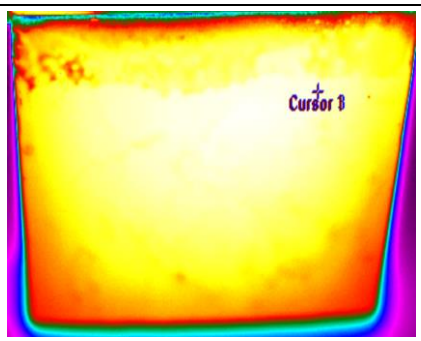	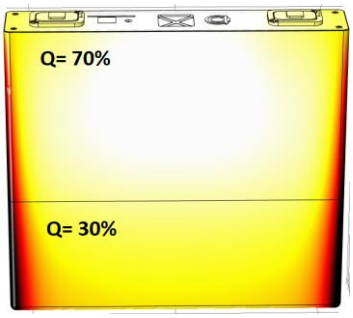
446	25	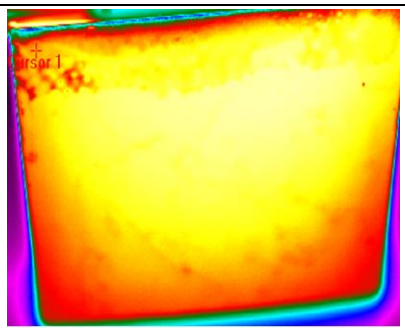	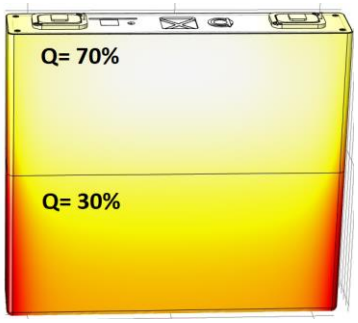
457	35	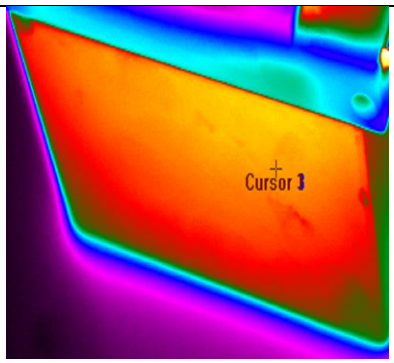	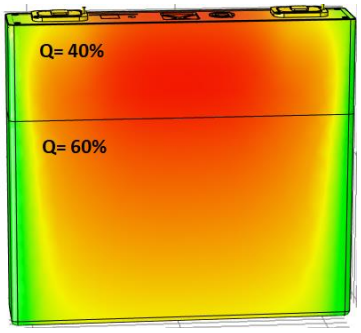

466	45	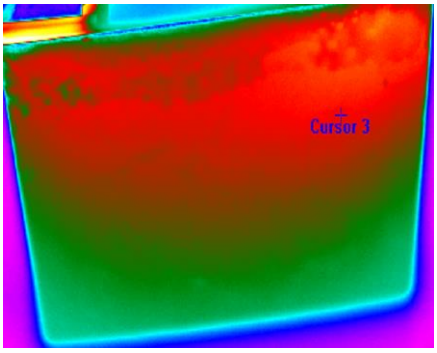	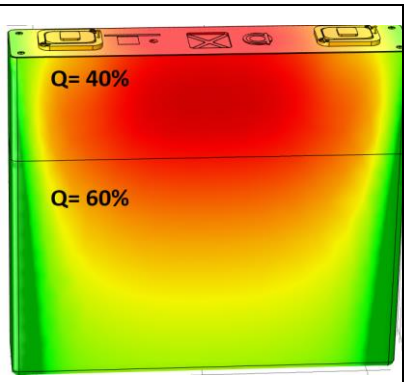
	Figure 42. Validation of the LTO 3D-thermal model at different initial temperatures at different simulation times		

4.5 Conclusion on the LTO modelling

The proper simulation of lithium-ion batteries in today's automotive and electric applications is of great importance for efficient use and correct understanding of the electrical, thermal, chemical behaviour of the system under investigation. Different models exist in the industry and literature, each having their own advantages and disadvantages. In this report, the development of a 1D-electro- thermal and 3D-thermal for predicting the thermal distribution and the voltage behaviour under static and dynamic load profiles of 23Ah prismatic cells is presented. The model, based on Matlab/Simulink and Comsol Multiphysics was elaborated on LTO cell. The experimental results used for validation showed a temperature estimation to be fairly uniform after a complete discharge with 2°C of maximal temperature difference. In addition, from the comparison of both simulations and the experimental results, a good agreement was found with a maximum error of 2 % and 2°C for the electrical and thermal. Additionally, the validation has been done at five initial temperatures (0°C, 10°C, 25°C, 35°C and 45°C) which means that a solid foundation for a generalized model methodology is provided. Therefore, with the dynamic and static validation profiles performed on this cell, a solid foundation for a generalized model methodology is provided.

5 Conclusion

In this report, a detailed understanding of the electro-thermal behavior of LTO 23 Ah batteries have been proposed. VUB characterization techniques in electric-thermal characterization have allowed in creating a good set of electrical and thermal parameters which can be implemented to perform electric and thermal model activities. The results of the electric-thermal characterization tests highly influence the outcome of the battery model. The type of tests are always the same but the difference comes in by way of careful implementation of the test itself, battery connections and intricate modifications

in the test protocols. Such dedicated modifications have led to the creation of a qualitative set of electro-thermal characterization tests at different C rates, State of Charge levels and temperatures.

The results of the characterization test of the LTO chemistry of the GHOST project were as expected and matches with the general information provided by the manufacturer data sheet. In the coming, section, the validation of these parameters will be presented in a modeling study for which a 1D-electro-thermal model is developed.

In this report, the development of a 1D-electro- thermal and 3D thermal model for predicting the thermal distribution and the voltage behavior under static and dynamic load profiles of 23Ah prismatic cells was presented. This model, based on Matlab/Simulink interface was elaborated on LTO cell. From the comparison of both simulations and the experimental results, a good agreement was found with a maximum error of 2 % (4 %) and 2°C for the electrical and thermal, respectively. Therefore, with the dynamic and static validation profiles performed on this cell, a solid foundation for a generalized model methodology is provided and can be used for WP8.

6 References

[1] I. Baghdadi, O. Briat, A. Eddahech, and J. M. Vinassa, “Electro-Thermal Model of Lithium-ion Batteries for Electrified Vehicles Applications,” *IEEE Int. Symp. Ind. Electron.*, pp. 1324–1328, 2015.

[2] N. Omar, P. Van Den Bossche, T. Coosemans, and J. Van Mierlo, “Peukert Revisited—Critical Appraisal and Need for Modification for Lithium-Ion Batteries,” *Energies*, pp. 5625–5641, 2013.

[3] J. Jaguemont, L. Boulon, and Y. Dubé, “A comprehensive review of lithium-ion batteries used in hybrid and electric vehicles at cold temperatures,” *Appl. Energy*, vol. 164, pp. 99–114, 2016.

[4] J. Jaguemont, L. Boulon, and Y. Dubé, “Characterization and modeling of a Hybrid Electric Vehicle Lithium – Ion Battery at Low Temperatures,” *IEEE Trans. Veh. Technol.*, vol. 65, no. 1, pp. 1–14, 2015.

[5] T. Huria, M. Ceraolo, J. Gazzarri, and R. Jackey, “High Fidelity Electrical Model with Thermal Dependence for Characterization and Simulation of High Power Lithium Battery Cells,” *IEEE Int. Electr. Veh. Conf.*, pp. 1–8, 2012.

[6] L. Boulon, D. Hissel, and M.-C. Pera, “Multi Physics Model of a Nickel Based Battery Suitable for Hybrid Electric Vehicle Simulation,” *J. Asian Electr. Veh.*, vol. 6, no. 2, pp. 1175–1180, 2008.

[7] J. De Hoog, J.-M. Timmermans, D. Ioan-Stroe, M. Swierczynski, J. Jaguemont, S. Goutam, N. Omar, J. Van Mierlo, and P. Van Den Bossche, “Combined cycling and calendar capacity fade modeling of a Nickel-Manganese-Cobalt Oxide Cell with real-life profile validation,” *Appl. Energy*, vol. 200, pp. 47–61, 2017.

[8] J. Jaguemont, L. Boulon, and Y. Dube, “Characterization and Modeling of a Hybrid-Electric-Vehicle Lithium-Ion Battery Pack at Low Temperatures,” *IEEE Trans. Veh. Technol.*, vol. 65, no. 1, pp. 1–14, 2016.

[9] F. P. Incropera and D. P. DeWitt, *Fundamentals of Heat and Mass Transfer*, Fifth. 2001.

7 Annex A

Table 15. R_0 values with temperature, SOC and C-rate.

Discharge																					
SOC	5	10	15	20	25	30	35	40	45	50	55	60	65	70	75	80	85	90	95	100	C-rate
0	0.003367	0.003271	0.003158	0.003089	0.003019	0.003019	0.002986	0.002933	0.00296	0.00289	0.002934	0.002925	0.002841	0.002853	0.002808	0.002852	0.002872	0.002827	0.002868	0.002732	C/3
	0.003275	0.003205	0.003159	0.003072	0.003031	0.002946	0.002898	0.002968	0.002907	0.002935	0.002919	0.002889	0.002894	0.002822	0.002844	0.00281	0.002825	0.002796	0.002825	0.002724	C/2
	0.003229	0.003166	0.003089	0.003018	0.002978	0.002936	0.002903	0.002883	0.002882	0.00286	0.002834	0.002839	0.002815	0.002798	0.002779	0.002763	0.002749	0.002741	0.002755	0.002658	1C
	0.00317	0.003076	0.003014	0.002952	0.002887	0.002866	0.002842	0.002809	0.002804	0.002789	0.002778	0.002763	0.002718	0.00273	0.002708	0.002702	0.002712	0.002709	0.002609	0.002586	1.5C
	0.003	0.003001	0.002922	0.002854	0.002813	0.00279	0.002747	0.002735	0.002716	0.002704	0.002709	0.002683	0.002672	0.002644	0.002644	0.002631	0.002642	0.002557	0.002535	0.002512	2C
10	0.002434	0.001534	0.001301	0.001102	0.001099	0.000892	0.001069	0.001026	0.00098	0.001297	0.001598	0.001847	0.001893	0.002037	0.00192	0.0017	0.001555	0.001675	0.001724	0.001747	C/3
	0.002572	0.001789	0.001457	0.00113	0.000999	0.000945	0.001005	0.001008	0.001139	0.001175	0.001699	0.00186	0.001954	0.001867	0.001808	0.001703	0.001693	0.001542	0.001543	0.001638	C/2
	0.003481	0.002122	0.001646	0.001371	0.001249	0.00123	0.001174	0.001155	0.001217	0.001345	0.001702	0.001948	0.002111	0.00204	0.00201	0.001865	0.001877	0.001697	0.001766	0.001696	1C
	0.004624	0.002297	0.00163	0.001354	0.001243	0.001175	0.001165	0.00111	0.001161	0.001245	0.001539	0.001909	0.001947	0.001941	0.001909	0.001794	0.001805	0.001794	0.001459	0.001428	1.5C
	0.005812	0.002663	0.001667	0.001372	0.001243	0.001191	0.001155	0.001122	0.001114	0.001178	0.001478	0.001775	0.001878	0.001854	0.001817	0.001775	0.001734	0.00114	0.001065	0.00099	2C
25	0.00132	0.001271	0.00125	0.001198	0.001232	0.001224	0.001187	0.001183	0.00121	0.001181	0.001229	0.001178	0.00118	0.001115	0.001107	0.001111	0.00112	0.001096	0.001117	0.001084	C/3
	0.001326	0.001271	0.001261	0.001201	0.0012	0.001182	0.001188	0.001219	0.00123	0.001202	0.001211	0.001171	0.001158	0.001146	0.001123	0.001108	0.001104	0.001141	0.001093	0.001089	C/2
	0.001308	0.001268	0.001254	0.001231	0.001204	0.001193	0.001196	0.001226	0.001225	0.001206	0.001218	0.001182	0.001176	0.001116	0.001118	0.001125	0.001118	0.001124	0.001126	0.001098	1C
	0.00131	0.001271	0.001244	0.001226	0.001202	0.001196	0.001184	0.001235	0.001226	0.001207	0.001204	0.001194	0.001177	0.001122	0.00112	0.001124	0.00111	0.00112	0.001102	0.001092	1.5C
	0.001301	0.001268	0.001243	0.001229	0.001205	0.001197	0.001178	0.001206	0.001209	0.001206	0.001203	0.001179	0.001175	0.001118	0.001111	0.001113	0.001117	0.001103	0.001093	0.001083	2C
45	0.002609	0.001421	0.00115	0.000996	0.000911	0.00088	0.000762	0.000874	0.000826	0.000691	0.00093	0.001306	0.001173	0.001024	0.000997	0.001091	0.001237	0.0012	0.00107	0.000916	C/3
	0.002587	0.001428	0.001225	0.000878	0.000869	0.000727	0.000751	0.000686	0.000732	0.000806	0.001036	0.001267	0.001067	0.00116	0.001309	0.001189	0.001245	0.001045	0.00104	0.000956	C/2
	0.002773	0.001334	0.001104	0.000981	0.000883	0.000835	0.000778	0.000743	0.000719	0.000723	0.000883	0.001217	0.001255	0.001213	0.001229	0.001161	0.001108	0.001043	0.001105	0.000927	1C
	0.002926	0.001263	0.001182	0.000961	0.000874	0.000816	0.000759	0.000743	0.000714	0.000713	0.000786	0.001206	0.001234	0.00126	0.001211	0.001185	0.001104	0.001016	0.00088	0.000856	1.5C
	0.002802	0.001033	0.000944	0.000844	0.000755	0.000752	0.00082	0.000636	0.000636	0.000818	0.000937	0.001135	0.001218	0.00126	0.001187	0.001153	0.001211	0.000958	0.000946	0.000934	2C
Charge																					
SOC	5	10	15	20	25	30	35	40	45	50	55	60	65	70	75	80	85	90	95	100	C-rate
0	0.003479	0.003368	0.003212	0.003139	0.00315	0.003108	0.003075	0.00309	0.003044	0.003041	0.003023	0.003053	0.00303	0.002965	0.00296	0.00291	0.002891	0.002918	0.002864	0.002815	C/3
	0.003421	0.003274	0.003219	0.003187	0.003061	0.003096	0.003009	0.00302	0.003045	0.002959	0.00299	0.002935	0.002946	0.002901	0.002868	0.002941	0.00288	0.002905	0.002915	0.002793	C/2
	0.003356	0.003258	0.003184	0.003116	0.003062	0.003012	0.003003	0.002975	0.002958	0.002953	0.002943	0.002916	0.0029	0.002884	0.00287	0.002847	0.002853	0.002837	0.002878	0.002753	1C
	0.003288	0.003205	0.003113	0.003064	0.00299	0.002969	0.002937	0.002914	0.002912	0.002885	0.002871	0.002863	0.002832	0.002843	0.002817	0.00281	0.002814	0.002795	0.002707	0.002683	1.5C
	0.0032	0.003109	0.00303	0.002969	0.002923	0.002911	0.00287	0.002849	0.002831	0.002816	0.002827	0.002792	0.002779	0.002765	0.002754	0.002749	0.002721	0.002654	0.002629	0.002605	2C
10	0.001815	0.001398	0.001183	0.000947	0.000882	0.000865	0.000782	0.000954	0.001011	0.001072	0.001256	0.001558	0.001733	0.001778	0.001372	0.001313	0.001528	0.001499	0.001658	0.001548	C/3
	0.001682	0.001249	0.00108	0.000989	0.000939	0.000967	0.000909	0.000978	0.001029	0.001075	0.001423	0.001649	0.001572	0.001587	0.001418	0.001401	0.001223	0.001298	0.001493	0.00145	C/2
	0.001419	0.001296	0.001263	0.001157	0.00094	0.001009	0.000934	0.000959	0.000997	0.001137	0.00147	0.001453	0.001376	0.00142	0.00126	0.001392	0.001304	0.001293	0.0001	0.001094	1C
	0.001423	0.001256	0.001126	0.001093	0.000958	0.000934	0.00097	0.000916	0.000989	0.001158	0.001481	0.001341	0.001296	0.001341	0.001365	0.001329	0.001374	0.001503	0.001395	0.001414	1.5C
	0.00129	0.001272	0.001087	0.001003	0.000907	0.000906	0.000895	0.000911	0.000997	0.001153	0.001487	0.001296	0.00127	0.001306	0.001296	0.001316	0.001397	0.00134	0.00136	0.001379	2C
25	0.001354	0.001309	0.001272	0.001227	0.001238	0.001207	0.001196	0.001201	0.001248	0.001202	0.001165	0.001217	0.001186	0.001141	0.001114	0.001185	0.001121	0.001142	0.00116	0.001111	C/3
	0.001336	0.001289	0.001249	0.001227	0.001215	0.001181	0.001176	0.001208	0.00129	0.001226	0.001201	0.001216	0.001181	0.001154	0.001139	0.001126	0.00111	0.001121	0.001138	0.001107	C/2
	0.001331	0.001277	0.001246	0.001222	0.001222	0.001204	0.001194	0.001224	0.00122	0.001245	0.001215	0.001205	0.001193	0.001141	0.001119	0.001122	0.001122	0.001119	0.001136	0.001105	1C
	0.001313	0.001288	0.001251	0.001237	0.001206	0.001196	0.001202	0.001234	0.00123	0.001228	0.001217	0.001191	0.00119	0.001142	0.001108	0.001142	0.001122	0.001129	0.001112	0.001102	1.5C
	0.001306	0.001273	0.001241	0.001227	0.001208	0.001199	0.001192	0.001223	0.001228	0.001226	0.001215	0.001197	0.00118	0.001122	0.001125	0.001123	0.001118	0.001115	0.001106	0.001096	2C
45	0.001308	0.001248	0.001254	0.001172	0.001111	0.001123	0.001099	0.001092	0.001093	0.001054	0.001046	0.001019	0.001036	0.001003	0.000959	0.000987	0.000895	0.000887	0.000848	0.00085	C/3
	0.001258	0.001239	0.001189	0.001179	0.001142	0.001102	0.001095	0.001071	0.001065	0.001026	0.001025	0.001034	0.000992	0.000987	0.001	0.000961	0.000928	0.00087	0.000899	0.000865	C/2
	0.001279	0.001234	0.001223	0.001176	0.001146	0.001137	0.00108	0.001068	0.001064	0.001047	0.001007	0.001015	0.000989	0.000997	0.000989	0.000943	0.000923	0.000908	0.00088	0.000856	1C
	0.001422	0.001357	0.001321	0.001272	0.001252	0.001216	0.001166	0.001144	0.001139	0.001123	0.001089	0.00109	0.001029	0.001057	0.001047	0.001026	0.001008	0.000974	0.000928	0.000905	1.5C
	0.001564	0.001506	0.001412	0.001334	0.001291	0.001251	0.001218	0.001191	0.001162	0.00113	0.001132	0.001116	0.001094	0.001075	0.001073	0.001051	0.001023	0.000942	0.000912	0.000882	2C

8 Annex B

In this section, some general information, screen shots and graphical images about the environment of Matlab/Simulink in order to simulate the GHOST electro-thermal model.

Figure 41 displays the GEIRI NMC model with the different features:

- Input validation profiles: in this section, validation profiles obtained from experimental data can be implemented. In this example, a current (“Inp”), voltage (“Tension”) and temperature profiles are loaded.
- Energy calculation: this block calculates the energy spent during the profile.
- Error calculation: These blocks calculates the model deviation by comparing the measured data (“Vmeas” or “T_meas”) with the simulation result (“Vbatt” and “Tbatt” for the voltage and temperature, respectively).
- Combined 1D-electro-thermal model: this block is the 1D-electro-thermal model. Inputs are the current, voltage, initial and ambient temperature. One switch is proposed for the SOC estimation. Indeed two SOC estimation algorithms are possible: the coulomb counting or the extended Kalman filtering. The second one is more accurate, but requires the measure voltage to function. The other switch is for the calculation of the heat generation, one way is with the measured voltage, and the other one is with the electrical parameters. If the measured voltage is not known, then this switch should stay at 1.

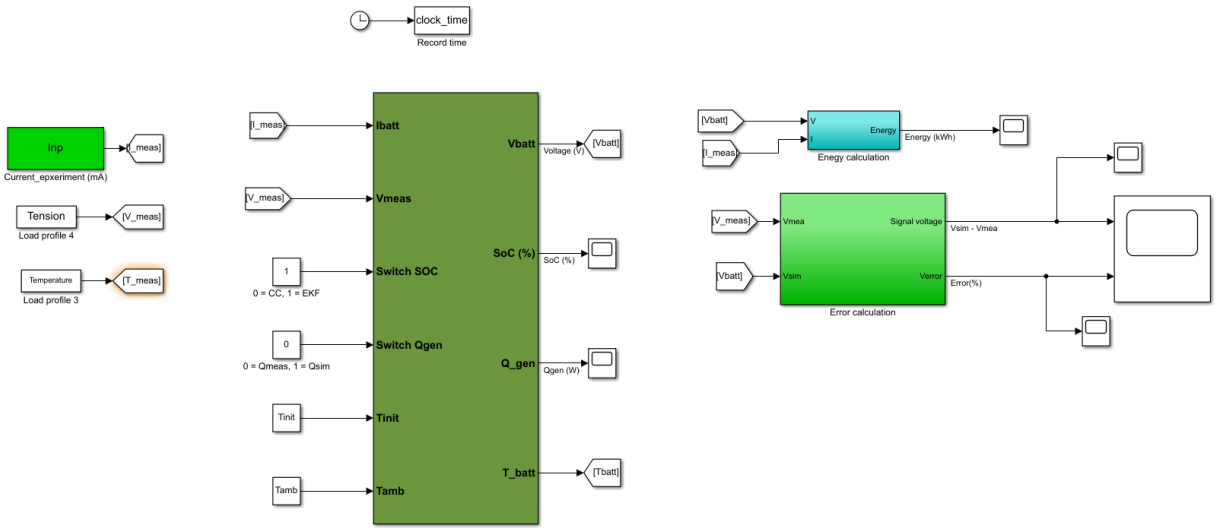

Figure 41. Matlab / Simulink model of the GHOST cell.

The model works in a Matlab / Simulink interface from Matlab 2019a. Figure displays this interface with the different features:

- Input validation profile: double-click on the validation profile, here called GHOST-LTO-8C-DCH-25degC_D.mat which is an 8C discharge at 25°C. The profile contains the time, temperature, voltage and current cycle.
- Model parameters: double-click on the parameter file, here called GHOST_parametersv3 which contains the electrical and thermal parameters in form of look-up tables.
- Simulink model: double-click on the model, here called GHOST_LTO_SP_2ndorder_final_v1 to open the Simulink model. Note that in order to function, two other files must be in the same folder as the model: GHOST_LTO_SP_2ndorder_final_v1_sfcn_rtw and GHOST_LTO_SP_2ndorder_final_v1_sf.

After that the parameters and the profile are loaded, the next step is to run the model. The time of the simulation is pre-determined with the time of the load profile called “Time”. If the user wants to reduce the simulation time, a constant value can be used in the model.

When the simulation is done, the results are transferred into the workspace and can be processed. Or they can display by double-clicking on the scope icons.

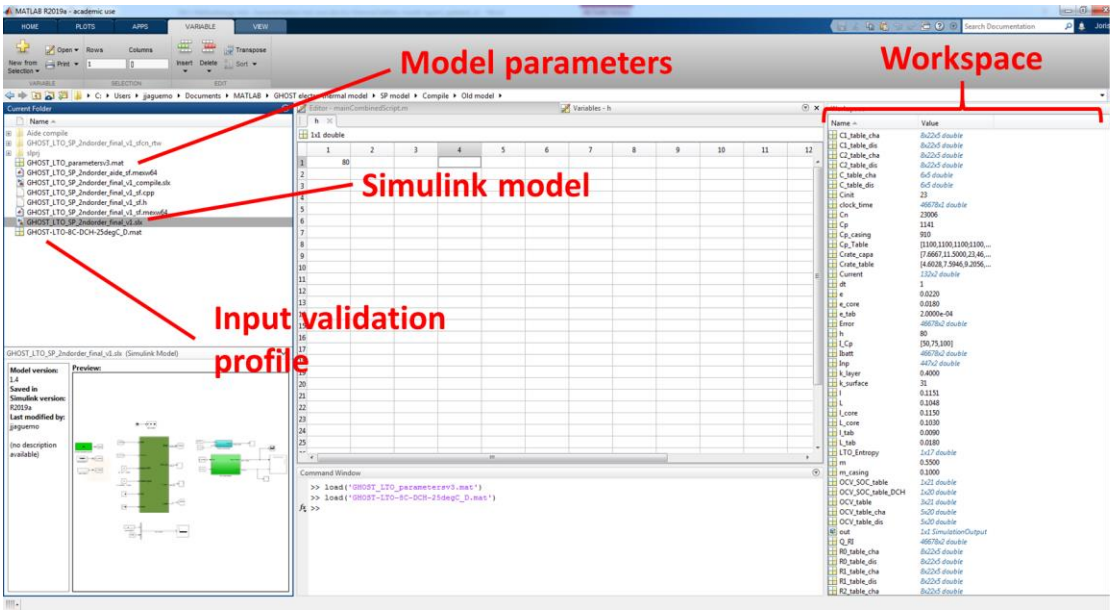

Figure 42. Matlab / Simulink interface.

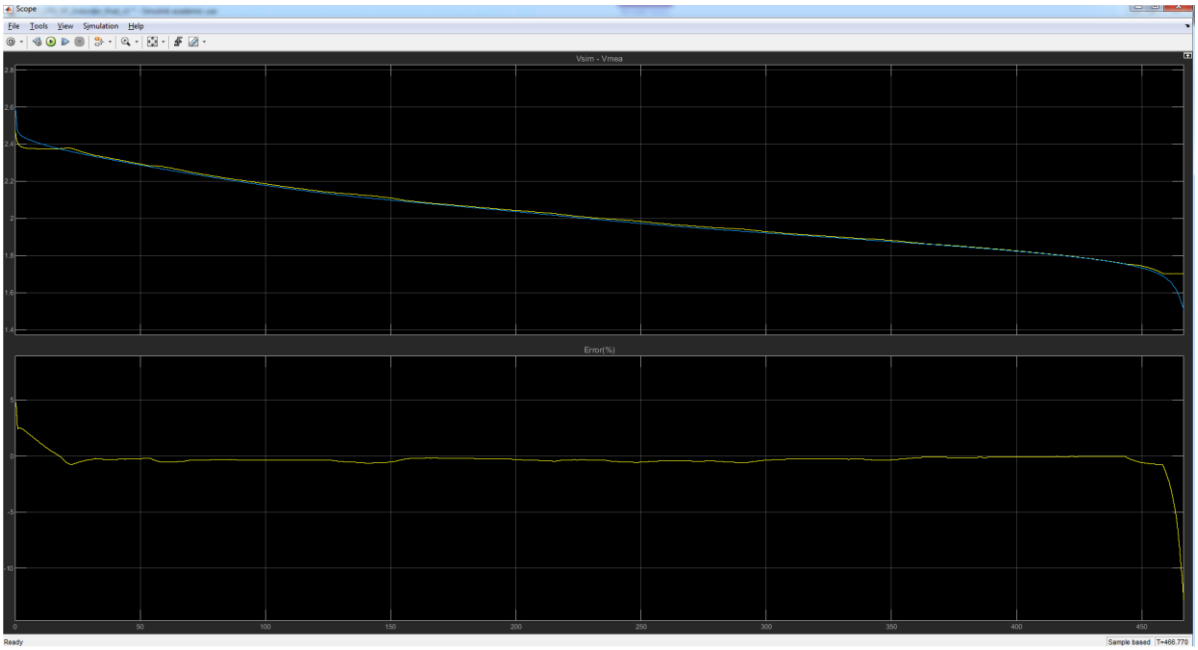

Figure 43. Electrical result of the LTO model